IAS SEDIMENTOLOGY
Journal of the International Association of Sedimentologists

Physical behaviour of Cretaceous calcareous nannofossil ooze: Insight from flume studies of disaggregated chalk

Journal:	*Sedimentology*
Manuscript ID	SED-2016-OM-012.R1
Manuscript Type:	Original Manuscript
Date Submitted by the Author:	n/a
Complete List of Authors:	Buls, Toms; University of Copenhagen, Centre for Cross-disciplinary Chalk Research (C3), Department of Geosciences and Natural Resource Management Anderskouv, Kresten; University of Copenhagen, Centre for Cross-disciplinary Chalk Research (C3), Department of Geosciences and Natural Resource Management Friend, Patrick; Pacific E&P USA Inc. Thompson, Charlotte; University of Southampton, School of Ocean and Earth Science Stemmerik, Lars; Natural History Museum of Denmark, Centre for Cross-disciplinary Chalk Research (C3)
Keywords:	Upper Cretaceous, experimental sedimentology, calcareous nannofossil ooze, chalk dynamics, flume, sediment transport

PHYSICAL BEHAVIOUR OF CRETACEOUS CALCAREOUS NANNOFOSSIL OOZE: INSIGHT FROM FLUME STUDIES OF DISAGGREGATED CHALK

TOMS BULS[1], KRESTEN ANDERSKOUV[1], PATRICK L. FRIEND[2], CHARLOTTE E. L. THOMPSON[3], LARS STEMMERIK[4]

[1]Centre for Cross-disciplinary Chalk Research (C3), Department of Geosciences and Natural Resource Management, University of Copenhagen, Øster Voldgade 10, DK-1350, Copenhagen K, Denmark

[2]Pacific E&P USA Inc., 5555 San Felipe St, Suite 1250, Houston, Texas 77056, USA

[3]School of Ocean and Earth Science, University of Southampton, National Oceanography Centre, Southampton, Hampshire SO14 3ZH, United Kingdom

[4]Centre for Cross-disciplinary Chalk Research (C3), Natural History Museum of Denmark, Øster Voldgade 5–7, DK-1350, Copenhagen K, Denmark

Corresponding author: Toms Buls (e-mail: toms.buls@gmail.com; Department of Geosciences and Natural Resource Management, University of Copenhagen, Øster Voldgade 10, DK-1350, Copenhagen K, Denmark).

Running title: PHYSICAL BEHAVIOUR OF CALCAREOUS NANNOFOSSIL OOZE

ABSTRACT

Geomorphic features such as drifts, sediment waves, and channels have been documented in the Upper Cretaceous of NW Europe. These features are interpreted to result from bottom currents and have been used to refine chalk depositional models and quantify paleocirculation patterns. Chalk was first deposited as calcareous nannofossil ooze and geomorphic features are the result of sediment reworking after deposition. There is limited knowledge on the processes that govern nannofossil ooze mobility, thus forcing uncertainty onto numerical models based on sedimentological observations. This paper provides an extensive view of the erosional and depositional behaviour of calcareous nannofossil ooze based on experimental work using annular flumes. A fundamental observation of this study is the significant decrease of nannofossil ooze mobility with decreasing bed porosity. Erosion characteristics, labelled as erosion types, vary with total bed porosity (φ) and applied shear stress (τ_0). High-porosity ooze ($\varphi > 80\%$) is characterized by constant erosion rates (E_m). At $\varphi < 77\%$, however, erosion characteristics showed greater variance. Surface erosion was typically followed by transitional erosion (with asymptotically decreasing E_m), and stages of erosion with constant, and exponential E_m. The estimated erosion thresholds (τ_c) vary from ~0.05–0.08 Pa for the onset of surface erosion and up to ~0.19 Pa for the onset of constant erosion (φ of 60–85%). Variability of deposition thresholds (τ_{cd}) from ~0.04–0.13 Pa reflects the influence of variable suspended sediment concentration (SSC) and τ_0 on settling particle size due to the identified potential for chalk ooze aggregation and flocculation. Additionally, τ_{cd} seem to be affected by the size of eroded aggregates whose size correlates with bed porosity. Lastly, slow sediment transport without resuspension occurred in high-porosity ooze as surface creep, forming low relief sedimentary features resembling ripples. This process represents a previously undescribed mode of fine-grained nannofossil ooze transport.

Keywords: Upper Cretaceous, experimental sedimentology, calcareous nannofossil ooze, chalk dynamics, flume, sediment transport

INTRODUCTION

The physical behaviour of calcareous nannofossil ooze has received relatively little attention, despite extensive deposition of fine-grained pelagic oozes during the Late Cretaceous and early Paleogene that led to the formation of thick successions of chalk over large areas of the world (*e.g.* Hancock, 1975; Håkansson et al., 1974). The chalk is composed mainly of debris of minute coccolithophorid algae deposited in deep-water shelf environments (*e.g.* Surlyk et al., 2003). Chalk deposition by slow pelagic settling of particles in the form of marine snow or faecal pellets under quiescent oceanic and tectonic conditions (Honjo, 1976; Steinmetz, 1994) formed evenly bedded, monotonous chalk facies. However, locally persistent bottom currents at the time of deposition contributed to sediment redistribution, leading to the formation of a variety of sedimentary features such as drifts, valleys, moats, channels, and sediment waves, as documented both onshore and offshore NW Europe (Anderskouv et al., 2007; Back et al., 2011; Esmerode et al., 2007; Esmerode et al., 2008; Esmerode and Surlyk, 2009; Gale et al., 2015; Gale et al., 2013; Gennaro and Wonham, 2014; Lykke-Andersen and Surlyk, 2004; Quine and Bosence, 1991; Surlyk et al., 2008; Surlyk and Lykke-Andersen, 2007). Episodic redeposition of chalk ooze as a result of downslope movement also occurred in areas experiencing syndepositional tectonic or halokinetic activity, resulting in submarine slides, slumps, debris-flows, mud-flows, grain-flows and turbidites (Anderskouv and Surlyk, 2011; Bramwell et al., 1999; Bromley and Ekdale, 1987; Campbell and Gravdal, 1995; Damholt and Surlyk, 2004; Hardman, 1982; Kennedy, 1987a; Kennedy, 1987b; Nygaard et al., 1983; Watts et al., 1980).

The commonly homogeneous appearance of the chalk due to its fine-grained texture and generally pervasive bioturbation imposes numerous challenges for the analysis and exploration of this important hydrocarbon reservoir and aquifer rock, and many aspects of the chalk dynamics, including deposition and redeposition are still poorly understood (*e.g.* Surlyk et al., 2003; Anderskouv and Surlyk, 2011, 2012).

As the chalk is an important hydrocarbon reservoir in the North Sea, the prediction of the distribution of key reservoir properties (*e.g.* porosity, permeability) within this rock is of particular interest. Multiple studies have noted a link between depositional processes and chalk porosity (Anderskouv and Surlyk, 2012; Campbell and Gravdal, 1995; Fabricius, 2007; Hardman, 1982; Kennedy, 1980; Kennedy, 1987a; Kennedy, 1987b; Nygaard et al., 1983). Advanced understanding of the physical behaviour of calcareous nannofossil

ooze will improve the understanding of chalk deposition by bottom currents or stochastic depositional events, which in turn may increase the predictability of facies and reservoir properties.

The influence of bottom currents on chalk deposition has been interpreted from seismic data (Esmerode et al., 2007; Esmerode et al., 2008; Esmerode and Surlyk, 2009; Lykke-Andersen and Surlyk, 2004; Surlyk et al., 2008; Surlyk and Lykke-Andersen, 2007; van der Molen et al., 2005) or stratigraphy and bedding geometries (Anderskouv et al., 2007; Gale et al., 2015; Gale et al., 2013; Jarvis, 2006; Quine and Bosence, 1991). However, it is not possible to quantify confidently the strength of the inferred bottom currents with the existing knowledge on nannofossil ooze mobility. This limits the refinement of depositional models and complicates the interpretation of palaeocirculation from the sediment record, thus forcing uncertainty onto numerical models based on sedimentological observations.

Although the sedimentary processes responsible for siliciclastic sediment and calcareous nannofossil ooze mobility are assumed to be similar, knowledge of the physical behaviour of the latter is comparatively limited. Current knowledge on calcareous sediment mobility is based on flume experiments using shallow-water, fine-grained skeletal carbonate sand and mud (Neumann et al., 1970; Prager et al., 1996; Schieber et al., 2013; Young and Mann, 1985), and foraminiferal oozes (Kontrovitz et al., 1979; Oehmig, 1993). Very few studies focus on the mobility of nannofossils that dominate pelagic calcareous oozes (Black et al., 2003; Southard et al., 1971). In addition, modern pelagic ooze used in the aforementioned studies is characterised by finer coccolith size (Herrmann and Thierstein, 2012) and generally higher clay content (> 20 wt %) than pure chalk ($CaCO_3$ > 98 wt %). These differences hinder mobility evaluation of pure calcareous nannofossil ooze because additional components (*e.g.* clay, organic matter, sponge spicules, a larger fraction of microfossils such as foraminifera) may influence the physical behaviour of the ooze through increased cohesiveness or coarseness of the sediment.

The aim of this paper is to provide an extended view on the erosional and depositional behaviour of pure Cretaceous calcareous nannofossil ooze. The study is based on experimental work using annular flumes, to evaluate the influence bed porosity plays in the mobility of increasingly consolidated sediments analogous with increasing burial depth. The following research questions address basic problems in chalk ooze

mobility: (1) Erodibility of high-porosity and variable-porosity beds; (2) Depositional behaviour under applied shear stress τ_0 and under still-water conditions; (3) Sub-resuspension threshold dynamics of the bed.

METHODS AND MATERIALS

Experimental sediment

Calcareous nannofossil ooze was prepared to fit specific criteria relevant for the study of Cretaceous chalk and its physical behaviour prior to consolidation. These criteria included: low-Mg calcite mineralogical composition, absence of organic matter, low concentration of non-carbonate material, low concentration of large macro- and microfossils, and grain size representative of Cretaceous nannofossils. The ooze was produced by employing the freeze-thaw fracturing method described by Buls et al. (2015) to disaggregate Upper Cretaceous chalk sampled in Sigerslev quarry, eastern Stevns Peninsula, Denmark. The chalk is of Maastrichtian age and belongs to the Møns Klint Formation (Surlyk et al., 2013). It is characterised by high total porosity φ (42–49 %), low non-carbonate (insoluble) residue of 1.4–1.7 wt % (Table 1) dominated mostly by smectite clay (Buls et al., 2015), and is generally very friable with little diagenetic alteration (Hjuler and Fabricius, 2009). The freeze-thaw disaggregation method was shown by Buls et al. (2015) to be an effective method for disaggregation of bulk chalk rocks into their nannofossil components, and the sediment produced using this method can be considered as the most appropriate Cretaceous model ooze for sedimentological experiments.

The dominant components of the experimental ooze are low-Mg calcite coccoliths and coccolith fragments, with a coarser fraction composed of microfossils such as foraminifera, calcispheres and pieces of small benthic fossils. The grain size of the sediment used in the experiments was sampled from the upper part of the bed within the flume and estimated using a particle laser-sizer Coulter LS 130 with a micro-volume module. To aid particle dispersion and deflocculation, a small amount of 5% sodium hexametaphosphate solution ($(NaPO_3)_6$, "Calgon") was added to the grain-size samples. Detailed characteristics of the experimental chalk ooze are given in Table 1. The average wet bulk density (ρ_b) and water content have been calculated from the known dry sediment weight and the bed volume in the flume. Total bed porosity (φ) was calculated according to Burdige (2006);

$$\rho_b = \varphi\rho_w + (1 - \varphi)\rho_s \qquad (1)$$

where ρ_w is water density and ρ_s is calcite grain density.

Experimental setup

Measurements of sediment mobility were carried out using two annular laboratory flumes at the National Oceanography Centre Southampton (NOCS), UK. The two flumes, Lab Carousel and Mini Flume, have different scales and geometries, but are particularly suited for these types of investigations due to their infinite flow lengths, which ensures the development of a full bottom boundary layer and retention of all suspended material.

Lab Carousel

The larger flume, Lab Carousel (Fig. 1 A), has a diameter of 2.0 m, a channel width of 0.15 m with maximum depth of 0.40 m, and a bed area of 0.872 m^2. The flume is built from acrylic plastic and has transparent base and sidewalls for visualisation during the experiments. A current in the flume channel is induced by eight equidistant paddles attached to a rotating lid, driven by a programmable electric motor. Measurements of the current velocity U take place in three dimensions (tangential (u), radial (v) and vertical (w)) using a *Nortek Vectrino* Acoustic Doppler Velocimeter (ADV), sampling at a rate of 25 Hz at a height ~0.01 m above the bed. The suspended sediment concentration (SSC) in the annulus is estimated using three *D&A Instruments* Optical Backscatter Sensors (OBS) located at 0.03, 0.10 and 0.20 m above the bed, logging at a rate of 1 Hz. Flow velocities during experiments in the Lab Carousel ranged from 0.05 to 0.60 m/s with flows being fully turbulent. Reynolds numbers (calculated for a rectangular duct) ranged from 10500 at 0.05 m/s to 125000 at 0.60 m/s. The flow properties in the Lab Carousel have been extensively studied (Thompson et al., 2003, 2004, 2006), and the flume has been used in multiple sediment mobility studies (*e.g.* Cloutier et al., 2002, 2006; Lefebvre et al., 2010).

Mini-Flume

The smaller Mini-Flume (Fig. 1 B) has a diameter of 0.305 m, a 0.045 m wide channel, and a bed area of 0.034 m^2. The maximum water depth used in the experiments was 0.22 m. The current is induced by a rotating lid with 4 equidistant paddles. The Mini-Flume motor speed (M) has been calibrated to current speed using *Nortek Vectrino* "side looking" ADV, with a sampling rate of 25 Hz. The M value is linearly related to the current speed *U* at 0.09 m above the flume base. Furthermore, the current speed *U* has been converted to bed shear stress τ_0 values. The Mini-Flume is equipped with three *D&A Instruments* OBS's (0.02, 0.09 and 0.2 m above base) and a sampling port at the height of the middle OBS for SSC calibration. Flow velocities in the Mini-Flume experiments ranged from 0.05 to 0.45 m/s, with flows being transitional to fully turbulent (corresponding Reynolds numbers 3600 to 32000). Multiple studies have been performed using the Mini-Flume and its in-situ analogue (*e.g.* Amos et al., 2000; Thompson et al., 2004; Widdows et al., 2007) .

Experimental procedure

A total of 32 experiments were performed addressing basic problems in chalk ooze mobility. All experiments used deionized water to which calcium-enriched salt (*FluvalSea*) was added to reach salinity of 35 g/l and pH > 8.0. Water temperature in the flumes varied approximately between 18–23 °C (room temperature). The collected OBS data have been calibrated against SSC using 50 ml water samples, taken from the water sampling ports located at corresponding OBS heights, following changes in turbidity during the experiment. Samples were filtered through pre-weighed 47 mm glass microfiber filters, oven-dried at 60° C and weighed to determine SSC. The sensitivity of the OBS's is limited to a maximum SSC of 2–3 g/l due to specific grain size and colour of the sediment particles. Experiments were therefore restricted to SSC below the saturation threshold of the OBS. The grain size of suspended particles has been estimated for several experiments in the Lab Carousel measuring the grain size variability during the erosion and deposition. The samples were taken from the flume channel at the middle OBS level after the onset of erosion.

High-porosity bed mobility

The mobility of high-porosity beds were investigated in both the Lab Carousel and Mini-Flume by testing the erosion of beds subjected to short consolidation times after settling from low-concentration suspensions. The flume was filled with a sediment–water mixture with a sediment concentration of 25 g/l in the Mini-Flume and 60 g/l in the Lab Carousel. The sediment was maintained in suspension and mixed for 30 min at flow velocities exceeding 0.60 m/s. The suspended sediment was then allowed to settle under still water conditions and consolidate for 4 or 24 h forming beds with total porosities ranging from 84.9 to 82.7 % (corresponding to wet bulk densities of 1280–1316 kg/m^3). In one case (run LC #8), the sediment was left to consolidate for 1 month to estimate the effect of an extended consolidation period on ooze mobility. The grain size of the sediment was measured using the top 3 cm of the bed and compared with sediment measured separately using a laser-particle sizer (Buls et al., 2015) (see comparison with "Original ooze" in Table 1). The results show that the coarse-grained sub-1 mm fraction was concentrated at the base of the flume due to differential settling velocity during the still-water phase. The succeeding experiments therefore only involved the fully disaggregated, fine-grained ooze and not residual, non-disaggregated chalk fragments.

Out of the total number of 32, 14 experiments studied high-porosity bed mobility. Five replicate experiments were carried out for each of the 4 h and 24 h consolidation experiments to evaluate the experimental error. Two additional experiments included extended length velocity steps and 1 month consolidation period. The experiments were based on stepwise increases of current velocity to define the erosion threshold τ_c (Fig. 2) using small velocity increments (~0.005 Pa; ~0.01 m/s) to precisely define the τ_c. The current velocity was sustained for 10 min after each step increment (typically 9–11 in total) and the same velocity increments were used in all experiments. After the onset of erosion, visible as an increasing cloudiness of the water column, the stepwise increase of flow velocity was continued until reaching levels close to saturation of the OBS, corresponding to SSC of 2–3 g/l. The maximum applied τ_0 was 0.06–0.07 Pa for the 4 h consolidation experiments, up to 0.08 Pa for the 24 h consolidation experiments and 0.10 Pa for a 1 month consolidation experiment. Deposition threshold τ_{cd} was estimated in 5 out of 14 experiments by a stepwise decrease

(typically 7 steps) of the flow velocity (Fig. 2). Mass settling velocities W_s were determined during a 10 min long still-water phase directly after the last velocity step.

Variable-porosity bed mobility

The influence of variable bed porosity on chalk ooze mobility was investigated only in Mini-Flume. Sediment beds with predefined porosity were constructed from a mixture of a known dry mass of sediment and a measured amount of water. The mixture was then placed in the flume and the bed surface was levelled to avoid any artificial variation in bed roughness that might influence resuspension. The flume was slowly filled with water, covering the bed with a layer of bubble wrap to avoid resuspension of the remoulded bed. Although, the prepared beds are assumed to have uniform properties, some disturbance of the bed surface during the surface smoothening and water-filling phase cannot be excluded. The ooze used in these experiments was first sieved through 212 µm sieves to avoid the presence of coarse, sub-1 mm size non-disaggregated chalk fragments, while retaining foraminifera (< 200 µm). This additional operation was necessary to ensure that the sediment would be comparable to sediment used in high-porosity bed mobility experiments where the coarse fraction was effectively removed due to differential settling in the still-water settling phase. The grain-size results show only a small fraction of particles larger than 20 µm (see "Variable-porosity ooze" in Table 1) and the largest particles do not exceed 80 µm ensuring that sediment with comparable grain size was used in all experiments. Experiments were conducted for beds with total porosities ranging from 82.2 to 59.9 % and corresponding wet bulk densities of 1325 to 1700 kg/m^3 (11 experiments in total). The experiment design is similar to the setup for experiments with high-porosity beds (Fig. 2) with typically 10 to 13 velocity increments to estimate the erosion threshold τ_c and 7 decreasing velocity steps to estimate the deposition threshold τ_{cd}. This was followed by a 10 min long still-water phase during which mass settling velocities W_s were determined. Extended experimental time and additional velocity steps were needed to reach equivalent levels of erosion (in terms of SSC) as beds with decreasing porosity were studied. The maximum applied τ_0 was from 0.10 Pa (φ = 82.2 % experiment) to 0.25 Pa (φ = 59.9 % experiment). Velocity increments of ~0.005 Pa (~0.01 m/s) were used up to τ_0 of 0.09 Pa to define

the surface erosion threshold τ_c. Above this value, larger velocity increments of ~0.018 Pa (~0.03 m/s) were used to study the development of bed erosion.

Deposition

Two experiments were conducted in the Lab Carousel to assess deposition dynamics under variable flow velocity over a smooth flume bed without sediment cover. This setup allows assessment of the deposition threshold τ_{cd} excluding potential simultaneous sediment entrainment due to erosion. A sediment–water mixture with initial SSC of either 0.9 or 1.7 g/l was subjected to flow velocities of ~0.60 m/s for 30 min followed by step-wise reduction of flow velocity in 14 steps (duration of each 10 min). Mass-settling velocities were estimated after each experiment during a still-water settling phase that followed the last velocity step. During the experiment, any changes in width of the deposited layer within the flume channel were recorded via time-lapse photography, accompanied by SSC records from the OBS's, allowing for comparison between timing of deposition at the sediment–water interface and net downward flux.
Three additional separate experiments were conducted to estimate the mass settling velocities W_s from different suspended sediment concentrations (0.9 and 1.7 g/l) for an extended still-water settling period. These experiments were conducted by mixing the sediment–water mixture at high flow velocities ~0.60 m/s (~0.23 Pa) for 30 min and then allowing the material to settle under still-water conditions for up to 78 min while recording SSC with the OBS's.

Sub-resuspension threshold sediment dynamics

Additional experiments were conducted to study sediment transport at the sediment–water interface at flow velocities below the resuspension threshold. We felt it was necessary to examine the mobility potential of very fine-grained nannofossil sediment without entrainment into suspension, especially since formation of small-scale migrating depositional bedforms in lime mud has been revealed in studies by Schieber et al. (2013). Two separate flume runs were conducted. The first followed the dynamic evolution of a bed that was left to settle from 25 g/l suspension and consolidate for 24 h in the Lab Carousel forming a bed with 84 % total porosity (ρ_b ~1295 kg/m^3). The second run was conducted in the Mini-Flume using a remoulded bed

with 78.8 % total porosity (ρ_b ~1385 kg/m^3). The first run used small flow velocity increments below the erosion threshold τ_c. Flow velocity was increased if no sediment was mobilised and reduced if signs of resuspension were noticed. The total experiment length was 8.5 h (5 velocity steps). The second experiment used a similar design and was conducted at comparatively higher flow velocities just below the threshold for surface erosion. The total length of the second experiment was 22 h using 3 velocity steps below and at surface erosion threshold τ_c values.

Data – processing and definitions

Bed shear stress

The ADVs record flow in 3 dimensions: u (along channel), v (across channel) and w (vertical). The bed shear stress τ_0 was determined by applying the turbulent kinetic energy (TKE) approach

$$\text{TKE} = \frac{1}{2}\rho_w(\overline{u'^2} + \overline{v'^2} + \overline{w'^2}) \qquad (2)$$

of Soulsby (1983), where u' indicates the fluctuating part of the instantaneous tangential velocity component u, derived by subtracting the mean velocity value $\bar{u}$ from the instantaneous velocity u, as follows $u' = \bar{u} - u$. The notation $\overline{u'^2}$ indicates the variance of the fluctuating part u'. The turbulent kinetic energy density TKE can be related to τ_0 through an empirical constant

$$\tau_0 = 0.19\text{TKE} \qquad (3)$$

(Stapleton and Huntley, 1995). The use of the TKE method for calculation of τ_0 has been considered as one of the most robust and reliable methods for assessing bed shear stress τ_0 (Kim et al., 2000; Pope et al., 2006; Thompson et al., 2003) and is especially applicable for annular flumes where secondary circulations necessitate the evaluation of all three flow components (Thompson et al., 2003).

Critical erosion thresholds

The critical erosion threshold τ_c (Pa) has been defined as the point of initiation of bed erosion at an applied bed shear stress τ_0: where the SSC values deviate from the initial pre-experiment (background) SSC values in the flume. It is determined through linear regression of 30 sec averaged SSC versus τ_0 data, solved for

average pre-experiment SSC value. The method, considered as reproducible and reliable, is detailed in studies by Sutherland et al. (1998) and Amos et al. (2003). It has been used to obtain τ_c in sandy and cohesive/adhesive muddy sediments (Amos et al., 2004; Thompson et al., 2013; Widdows et al., 2007). However, for the Mini-Flume experiments with variable-porosity beds, the fitting of this trendline yielded very low correlation coefficient values due to different erosion types, and the threshold for erosion is therefore defined as a value between the velocity steps at which the onset of erosion was observed. To investigate the influence of the chosen duration of the velocity steps (10 min) on the obtained bed erosion threshold τ_c values, we conducted an additional experiment using extended length velocity steps of 20 min. The results from this run are in accordance with runs using 10 min step lengths, thus validating the use of the shorter step lengths.

Erosion rates, erosion types and depth of erosion

The mean erosion rate E_m (kg/m^2/s) of the 30 sec averaged data was calculated following Amos et al. (2003)

$$E_m = \frac{\delta M}{\delta t} = \frac{V(SSC_{end} - SSC_{start})}{\Delta t A} \qquad (4)$$

where A is the flume footprint area and V is the flume volume.

An equivalent depth of erosion z_e (mm) was calculated after Thompson et al. (2011) where M is the total amount of dry material in suspension

$$\frac{dz_e}{dt} = \frac{dM}{dt}\frac{1}{A\rho_b} \qquad (5)$$

Erosion rates E_m have been used to identify the transition between the different erosion types and to assist in defining thresholds for the onset of particular types of erosion. The type of erosion was determined from trends in the erosion rate E_m through time (10 min velocity step).

Different erosion types help in describing the process of erosion and Tolhurst et al. (2009) define five erosion patterns in muddy sediment: Type Ia and Type II surface erosion, Type Ib surface erosion, transitional Type I/II and Type II mass erosion. Type I erosion is depth-limited and characterised by erosion rates E_m that peak rapidly once the erosion process starts and diminish with time reaching zero under the same applied shear stress τ_0 (Amos et al., 1996). According to Mehta and Partheniades (1982) this erosion

type is characteristic for stratified sediment beds, in which erodibility decreases with depth. The Type I erosion is subdivided into two modes: 1) erosion of high porosity surface layers of organic detritus (Type Ia) that might occur even under the lowest applied shear stress τ_0; and 2) erosion of the aggregated material that comprises the underlying bed (Type Ib). Both are labelled as "surface phenomenon" by Amos et al. (1992) and "surface erosion" by Tolhurst et al. (2009) due to their occurrence at the initial stages of erosion under low and intermediate applied stresses. As defined by Mehta and Partheniades (1982), surface erosion involves floc-by-floc rupture and entrainment of the surficial sediment . Type II erosion characterise uniform bed erosion with increasing depth, displayed as a constant erosion rate E_m at the same applied shear stress τ_0. A transitional phase between Type I and Type II erosion (Type I/II) described by Amos et al. (1997) may develop under high applied stress and can be defined as non-equilibrium form of Type I erosion. It is typically asymptotical and fails to reach equilibrium during the extent of the velocity step. Type II erosion typically occurs at the highest applied shear stresses τ_0, and is the final stage in bed erosion. It is characterised by a release and entrainment of large bed aggregates as a result of enlargement of surface irregularities (Amos et al., 1997; Tolhurst et al., 2009). Both Type I/II and Type II erosion are considered as bulk or mass erosion (Tolhurst et al., 2009). It results from a dynamic shear loading of the bed where the plane of failure lies deep within the bed, and failure leads to an almost immediate entrainment of the sediment above the plane (Mehta and Partheniades, 1982). Along with Type Ia and Ib surface erosion, Tolhurst et al. (2009) describe an additional surface erosion pattern in the form of Type II surface erosion. Both Type Ia and Type II surface erosion appear characteristic for loose, organic surface sediment under low τ_0 with the only distinguishing feature between them being the diminishing (Type Ia erosion) and constant (Type II surface erosion) erosion rate E_m with depth. In this study both patterns of surface erosion have been observed. However, the above mentioned Type Ib and Type II surface erosion describe erosion of an organomineral fluff layer, not characteristic for this study. To avoid confusion, the observed erosion patterns of loose surface sediment under low τ_0 with average E_m between 10^{-5} and 10^{-6} kg/m^2/s here is labelled as Type Is and Type IIs.

Deposition threshold and mass settling rate

The deposition threshold τ_{cd} is defined as the shear stress τ_0 at which material begins to drop back to the bed, and was determined following the experimental design and procedures of Amos et al. (2004). It is assumed that the settling of mud under applied τ_0 follows an exponential decay law

$$SSC(t) = SSC_{start}e^{-kt} \qquad (6)$$

Following this, each step of settling under applied τ_0 (see Fig. 2 for the experiment design) was evaluated by fitting an exponential decay equation to the SSC time-series to determine the decay constant *k*. The decay constant *k* is then plotted against the τ_0 for every decreasing velocity step. The deposition threshold τ_{cd} is determined by relating *k* to τ_0 (see Fig. 9) and regressing k to 0 (Amos et al., 2004).

The still water mass settling rate W_s (m/s) has been calculated from the rate of change in SSC in the flume (Amos et al., 1998)

$$W_s = \frac{\delta M}{\delta t}\frac{1}{SSC(t)} \qquad (7)$$

Deposition rate D_m is calculated from the rate of change in SSC following Amos et al. (2003). The equivalent sedimentation diameter D_s has been calculated from W_s following Gibbs et al. (1971).

RESULTS

Erosion thresholds and rates for high-porosity beds

The main variable in the experiments was the pre-experiment consolidation time. A summary of the experiments using variable pre-experiment consolidation intervals is presented in Table 2. A time-series example of the conducted experiments in Fig. 3 illustrates the slight delay in the timing of the onset of erosion, and reduction in erosion rates E_m for a given velocity step as the consolidation time increases. The slightly higher degree of consolidation recorded in the Lab Carousel experiments is reflected by a rather insignificant increase of erosion threshold τ_c (within the variance of the replicates) when compared to the Mini-Flume, with an average τ_c of 0.049 Pa and 0.050 Pa (for 4 h and 24 h consolidation experiments, respectively).

Type II erosion (Tolhurst et al., 2009) occurred in all high-porosity bed experiments. It was characterised by a linear increase in SSC and a constant rate of erosion (Fig. 3 B, C). The average E_m of 4.0–4.3 x 10^{-4} kg/m^2/s at the maximum applied τ_0 are similar for the two sets of consolidation experiments. However, higher applied τ_0 is required for lower porosity beds in the 24 h consolidation experiment to reach the same rate of erosion as in the 4 h consolidation experiment (Table 2). E_m and z_e both display positive linear relationships with excess τ_0 (Table 2), and E_m and z_e plotted against excess τ_0 show two linear trends, with the best fit being between z_e and excess τ_0 (Fig. 4). The linear trends show that even a small decrease in porosity (~1 %) due to consolidation has impact on the rate at which the erosion continues once the erosion threshold τ_c is exceeded. This slight difference in consolidation may translate into ~40% lower erosion rates E_m with an increase of excess τ_0 by 0.025 Pa (~0.05 m/s).

An obvious exception in the data is the 1 month consolidation experiment. This experiment was conducted in the Lab Carousel, following the same procedure and using the same sediment as in the 24 h consolidation experiment. Despite consolidation that reaches the same level (φ = 83.6 %; ρ_b = 1301 kg/m^3) as the surface ooze after 24 h, the overall erodibility of the sediment bed after 1 month consolidation was comparatively much lower (Table 2). The onset of erosion started at a slightly higher shear stress τ_0 (Fig. 3), with highest recorded τ_c of 0.057 Pa. Erosion rates E_m are 1.5 x 10^{-4} kg/m^2/s at the maximum excess τ_0 of 0.044 Pa (~0.09 m/s), and display a logarithmic relationship with excess τ_0 (Fig. 4). This indicates increasing bed stability

with depth and could indicate a transition from constant Type II to transitional Type I/II erosion (Fig. 3 C, last velocity step).

In our experiments, further consolidation with increasing consolidation time after 24 h indicated by bed thickness changes was not observed. Therefore, other factors contributing to the resulting increased bed stability after a 1 month consolidation period must be considered. One potential cause may be local cementation of ooze particles through precipitation of $CaCO_3$ in the pore space. The $CaCO_3$ saturated (> 300 mg/l, pH > 8.0) water would prevent any dissolution of existing calcite particles, and the combination of an extended period of quiescence and simultaneous H_2O evaporation from the flume may have triggered cementation. Biological stabilization of the bed is an unlikely scenario due to the use of deionized water and chalk ooze devoid of organic matter and because the bed was only strengthened at depth. Also, there is no visual evidence of any biological activity, which is commonly accompanied by discoloration.

Experiments revealed that slightly longer consolidation time (24 h versus 4 h) resulted in an insignificant increase (within the variance of replicates) of the erosion threshold τ_c, but a significant decrease in erosion rates E_m (Table 2). Thus, the surface of the bed will cease to consolidate shortly after deposition, whereas more deeply buried sediment will continue to consolidate as a result of the weight of the overburden. However, erosion of the high-porosity beds in our experiments occurred only as Type II linear erosion, characteristic of uniform-strength beds, which is probably due to the high erodibility of the high-porosity chalk ooze. Therefore even smaller velocity increments would be required to register minor changes in bed erodibility and Type I erosion.

Erosion thresholds and rates for variable-porosity beds

The threshold for surface erosion varied from 0.061 Pa to 0.081 Pa for the studied range of bed porosities (Table 3). It increases with decreasing bed porosity φ down to 71.8 % (ρ_b = 1500 kg/m^3) at which point further decrease in φ no longer equate to an increase in the initial (Type Is or IIs) threshold. Despite this, marked differences are seen in erosion type and the rate at which chalk ooze beds of different density are eroded (see Fig. 5).

The transition between different types of erosion has been recorded for all experiments as follows: 1) In Type Is or Type IIs erosion ("s" indicates surface erosion) the onset of erosion is characterised by very low erosion rates E_m that are either constant (showing linear increases in SSC with time that is characteristic of Type II erosion) or diminishing with time. The latter displays an asymptotic pattern in the SSC time-series and distinct peaks in E_m that quickly decrease to zero (the pattern generally characteristic for Type I erosion). 2) The initial phase is followed by the occurrence of a marked peak in erosion rate E_m at the beginning of each velocity increment, after which E_m asymptotically decreases, in many cases reaching values close to zero by the end of the velocity step (*e.g.* 30 to 60 minutes in Fig. 5 C). In the SSC time-series, this is reflected as a "stepwise-like" pattern of SSC values, which combined with comparatively higher erosion rates E_m distinguish the erosion pattern from Type Is and IIs. It is labelled as Type I/II, being a transitional type between surface erosion and constant (Type II) erosion. Given its asymptotical character, this erosion type may prove to be Type I with extended length of the velocity steps. In none of the experiments, however, did erosion cease at the end of any velocity increment, thus we avoided labelling it as Type I. 3) Following increasing velocity, Type I/II erosion is succeeded by Type II erosion (Table 3). Type II erosion is characterised by constant erosion rates E_m and the absence of pronounced peak erosion (*e.g.* minutes 90 to 110 in Fig. 5 C). It follows a linear trend in SSC and typically shows a significant increase of E_m compared to the previous erosion types (Table 3). Typically only one velocity step in each experiment displays this particular type of erosion, due to the reduced resolution caused by the larger velocity increments in the latter part of experiments. 4) The final erosion type is characterised by rapid, continuously increasing erosion throughout the velocity step (*e.g.* minutes 110 to 120 in Fig. 5 C). It is observed in the last velocity step in all experiments where porosities are below 77.7 % (ρ_b = 1400 kg/m^3). In the experimental time-series, this erosion can be easily distinguished because the SSC data follow an exponential trend under the same applied τ_0 (Fig. 5 B). This type of erosion has not been described from other sediment dynamics experiments and is here referred to as Type III erosion.

By defining the onset of each type of erosion as the erosion threshold τ_c, it is possible to make a detailed characterisation of the bed erosion development with increasing applied shear stress τ_0 and decreasing bed porosity φ (Fig. 6, 7). From the figures, it is apparent that marked differences in the actual τ_0 are required to

initiate significant erosion of ~1.0 x 10^{-4} kg/m^2/s, which is a level of erosion comparable to E_m at the onset of erosion in experiments using high-porosity beds (see Fig. 4). Significant erosion here is defined as the onset of Type II erosion because surface erosion affects only the uppermost few microns of the bed surface (Fig. 5 D). Surface erosion occurred sporadically and predominantly along the outer side of the flume in the form of small clouds of sediment (representing the bursting process). The rate of surface erosion varied between an average of 9.4 x 10^{-6} kg/m^2/s for less consolidated beds (φ > 71.8 %) and 5.2 x 10^{-6} kg/m^2/s for more consolidated beds (φ < 71.8 %) at applied τ_0 range 0.063–0.085 Pa. Significantly higher levels of erosion (Fig. 7) occurred after exceeding the threshold for Type I/II erosion ranging between 0.081–0.097 Pa with average E_m of 1.9 x 10^{-4} kg/m^2/s (φ > 71.8 %) and 2.8 x 10^{-5} kg/m^2/s (φ < 71.8 %). The range of τ_0 under which this type of erosion was observed increases with decreasing bed porosity φ, with the onset of subsequent Type II erosion happening at progressively higher τ_0 ranging from 0.112–0.186 Pa (Fig. 6). E_m values prior to the onset of exponential erosion were on average up to 3.5 x 10^{-4} kg/m^2/s for φ > 71.8 % (τ_0 < 0.15 Pa; see Fig. 7) and 8.0 x 10^{-5} kg/m^2/s for beds with φ < 71.8 % (τ_0 > 0.15 Pa). Thus, a general pattern of decreasing erosion intensity with decreasing bed porosity φ was observed (Fig. 7), with much higher applied τ_0 required to reach the same level of erosion. Exponential Type III erosion was observed in beds with φ < 77.7 % (ρ_b > 1400 kg/m^3), with threshold values for this erosion type varying between 0.129–0.221 Pa (Fig. 6). The erosion rates E_m after the onset of this erosion type were on average 5.1 x 10^{-4} kg/m^2/s for φ > 71.8 % (τ_0 < 0.17 Pa) and 3.1 x 10^{-4} kg/m^2/s for φ < 71.8 % (τ_0 > 0.17 Pa).

Deposition thresholds and still water deposition

The applied shear stress τ_0 values at which the suspended material begins to deposit were estimated in the Lab-Carousel and Mini-Flume from suspended sediment concentrations < 2 g/l. Two experiments tested deposition under variable applied τ_0 on a smooth flume floor using initial concentrations of 0.9 g/l and 1.7 g/l (Fig. 8). The experiment time series (Fig. 8 B) show an initial noticeable decrease of SSC beginning at the second (τ_0 ~0.13 Pa) and third (τ_0 ~0.08 Pa) applied shear stress τ_0 steps for starting SSC of 1.7 g/l and 0.9 g/l accordingly. A small amount of settled material was already visible on the flume floor during the first step as a very thin sediment band of irregular width (up to 0.2–0.5 cm) along the inner side of the flume wall. It was

constantly migrating along the inner side of the flume, and kept a constant width above 0.08 Pa. With decreasing τ_0 values < 0.08 Pa, the width of the band of deposited material steadily increased until a critical point where material was almost instantly deposited over the entire width of the flume. This point was reached at τ_0 of ~0.035 Pa (Fig. 8 D).

The coarsest chalk ooze fraction (> 20 μm) settled first, at applied τ_0 > 0.10 Pa. This material forms less than 2% of the sediment mass on average (Table 1; "Variable-porosity ooze") and most likely contains fragments of foraminifera and larger macrofossils, along with a potentially non-disaggregated chalk fragments. A slight difference between the settling rates of material being deposited from different starting SSC values is apparent (Fig. 8). This is demonstrated by a more rapid decrease in SSC values from the 1.7 g/l suspension, a comparably higher amount of material settling at the same applied shear stress τ_0 (Fig. 8 C), and a consequently wider sediment band on the flume floor (Fig. 8 D). To exclude the coarsest grains (potentially non-disaggregated chalk) and estimate the deposition threshold τ_{cd} for particles < 20 μm, the first 2% of deposited material is excluded from the τ_0 vs k (decay constant) plot (Fig. 9) assuming that the coarsest calcite grains will settle first. The estimated τ_{cd} (Fig. 9) range from ~0.06 Pa to ~0.08 Pa (for deposition from 0.9 g/l and 1.7 g/l suspensions, respectively). It should be noted that these deposition thresholds τ_{cd} are at the same range as the surface erosion thresholds τ_c, and the threshold for net deposition is estimated at ~0.035 Pa (compare Fig. 8 A and 8 D).

Deposition thresholds τ_{cd} that were estimated in combined erosion–deposition experiments (see the experiment design in Fig. 2) show a rather wide range. Deposition threshold τ_{cd} values vary between 0.04 Pa and 0.06 Pa in experiments with high-porosity ooze. In experiments with variable-porosity ooze bed these were between 0.07 Pa and 0.13 Pa (Table 4). Deposition thresholds τ_{cd} for the high-porosity ooze are of the same magnitude or lower than the threshold for erosion (see Tables 2 and 4). However, for run LC#8 (1 month consolidation) and in experiments with variable-porosity beds in general, the τ_{cd} is above that of the surface erosion (Type Is or IIs) threshold (see Tables 3 and 4). Compared to the onset of different types of erosion (Fig. 6), the shear stress τ_0 values of the deposition thresholds τ_{cd} are within the range at which the prevalent type of erosion is Type I/II. It should be noted that τ_{cd} are derived from OBS data and illustrate net deposition.

Mass settling velocity W_s (m/s) was estimated after the mobility experiments, during a 10 min still water settling phase in the Lab Carousel and Mini-Flume (Table 4). In addition, experiments with extended still-water phase up to 78 min were performed (Fig. 10). For these experiments, settling occurred over a smooth flume base without sediment cover and the experiment consisted of a mixing phase and a still-water settling phase. During the mixing phase, the sediment–water mixture (with SSC of 0.9 g/l and 1.7 g/l) was mixed at high velocity (~0.60 m/s or ~0.23 Pa) for 30 min followed by a settling phase.

Very slow settling occurred during the first 7–8 min after stopping the motor driving the paddles. During this phase, the flume conditions are in a state of transition from turbulent to still water conditions and this is the time it takes the settling material to pass the upper OBS. Within this transitional phase, the settling of the largest particles occurs, totalling to 4–32 wt% and indicating that the coarsest chalk ooze particles (> 20 μm; Table 1) will fall out from suspension during this phase. The initial transitional phase is succeeded by a rapid settling phase that lasts up to 10 min and is followed by slower settling taking a loglinear form (Fig. 10). The W_s values during the rapid settling phase (Fig. 11 A) are on average $5.8 \pm 2.2 \times 10^{-4}$ m/s (Table 4). The variations in settling rates are much smaller for the slow settling phase with W_s values between 2.4×10^{-4} m/s and 6.6×10^{-4} m/s, with an average of $3.7 \pm 1.0 \times 10^{-4}$ m/s (Fig. 11 A). The considerable scatter of W_s values in general seems to be unrelated to the SSC (Fig. 11 B). However, a positive relationship seems to exist between higher initial SSC values of the sediment-water mixture at the mixing phase and higher deposition rates D_m during the rapid settling phase (compare runs LC #9 and #13, in Fig. 10 A, B). In Figure 11 A (coloured dots), the highest W_s values are for particles in experiments where the initial sediment-water mixture was 1.7 g/l (*e.g.* run LC #13, in Fig. 11 A) during the mixing phase. Considerably lower W_s values were observed for experiments with a starting concentration of 0.9 g/l during the mixing phase (*e.g.* run LC #9; in Fig. 11 A).

Equivalent sedimentation diameter D_s for grains has been estimated after Gibbs et al. (1971) assuming grains of calcite density (2710 kg/m^3). The average grain diameter of settling particles ranges from 19 μm to 37 μm, with an average of 26 ± 5 μm (Table 4) for the rapid settling phase. The average equivalent grain size of particles settling during the slow settling phase is 21 ± 3 μm.

Suspended grain size variation

Samples of suspended sediment were taken to determine grain size of suspended primary particles during the experiments on the mobility of high-porosity beds after 24 h consolidation. This was done in order to possibly aid in identification of flocculation and aggregation, and selective sorting under low applied shear stress τ_0 in calcareous nannofossil sediments further investigating the cohesive nature of this type of sediment. Variations in suspended grain size were observed with changes in τ_0 and suspended sediment concentration. Mean grain size variations are between 5.8 and 15.8 μm (D_{50} 5.3–12.5 μm), with the primary particle diameter averaging 11.2 μm at the onset of erosion at τ_0 0.05–0.06 Pa, and 8.1 μm at τ_0 0.06–0.08 Pa. Generally, primary particle grain size decreases with increasing erosional depth (see Fig. 12 B). Thus, increasing shear stress τ_0 is accompanied by introduction of finer primary particles into suspension (see Fig. 12 C). During the last velocity step (0.07–0.08 Pa) of the erosion phase (Fig. 12 C), the mean grain size of suspended particulate material was 7.3 ± 0.8 μm (D_{50} 6.6 ± 0.7 μm).

An increase of the suspended particle size with decreasing current velocity (*e.g.* minutes 135 to 180 in Fig. 12 A) was observed at the end of the deposition phase. The measured grain size during this phase varied between 7–12 μm, with an average of 8.6 ± 1.6 μm reflecting increasing grain size after reaching maximum erosion depth during the erosion phase.

Sub-resuspension threshold sediment dynamics

Two experiments were conducted to study bed surface sediment transport at sub-resuspension threshold current velocities. The first experiment was conducted in the Lab Carousel on a bed with ~84 % porosity (ρ_b ~1295 kg/m^3) which had consolidated for 24 h. The current velocity was increased in a stepwise fashion. During the first step (τ_0 < 0.02 Pa, 0.08–0.09 m/s) a gradual, almost unnoticeable movement of the topmost few mm of the bed started to occur, forming a slightly uneven bed surface. Subsequently, a low-relief sedimentary feature developed with crescent shape in plan view that continuously migrated in the current direction at the inner side of the flume. Simultaneously, striations up to a few centimetres in length and oriented parallel and oblique to the current started to develop along the outer part of the flume channel (Fig. 13 B). Time-lapse photography revealed a slow downstream migration of sediment at 0.9 cm/h. At the

second velocity increment (τ_0 = 0.02 Pa; 0.10–0.11 m/s), the removal of the topmost part of the bed surface continued. The removed material was transported to the inner side of the flume at a rate of 3.8 cm/h without resuspension. Here, in a 5 cm wide zone, the ooze formed continuously migrating features with sinusoidal crests that were less than 0.2 cm high and 2.5–3.5 cm apart (Fig. 13 C). The succeeding third velocity increment (τ_0 = 0.03 Pa; 0.12–0.13 m/s) resulted in a continuous development of similar features that increased in wavelength (4–5 cm between the crests) and height (up to 0.5 cm) as even more material from the top most part of the bed was mobilised. These features developed along the entire width of the flume except for a narrow zone along the outer part of the flume where the bed was featureless. The low-relief sinusoidal and isolated crests were migrating at a rate of 6–12 cm/h (Fig. 13 D). After increasing velocity to τ_0 = 0.034 Pa (0.15–0.16 m/s), the previously formed features were rapidly flattened-out, leaving an even bed surface (Fig. 13 E), with some material entrained directly into suspension via bursting processes. By decreasing the current speed to previous velocity values (τ_0 = 0.02 Pa; 0.10–0.11 m/s), the formation of sedimentary features resumed. They reached up to 0.5 cm height, with wavelengths of 5–8 cm, and the sinusoidal and isolated crests migrated at a rate of 2.0–2.5 cm/h (Fig. 13 F).

It was not possible to recreate this mode of transport in experiments with lower porosity beds of ~78.8 % (ρ_b ~1385 kg/m^3) in the Mini-Flume. Sediment transport was not observed below the erosion threshold τ_c and further velocity increments at the τ_c level initiated slow erosion with material being carried directly into suspension.

DISCUSSION

Erosion thresholds and rates for high-porosity beds

Experiments by Black et al. (2003) showed clouding of the water column indicating the onset of surface erosion at very low shear stress τ_0 values (< 0.02 Pa). In contrast, our experiments did not show sediment entrainment at values below the resuspension threshold in high-porosity beds (~0.05 Pa). Black et al. (2003) attributed the almost immediate erosion of the surface ooze to grain sorting whereby the coccolith-size grains (fraction ~5–15 μm) were eroded before larger grains. Considering that the calcareous nannofossil ooze used in our experiments is entirely dominated by this fraction (up to ~91 vol %; Table 1), its comparatively lower

erodibility in our experiments may be attributed to a slightly higher level of sediment cohesiveness as the material is more homogeneous compared to the bimodal and generally coarser modern-day sediment used by Black et al. (2003). The low threshold for entrainment of coccolith-size particles demonstrated by Black et al. (2003) represents the surface erosion threshold τ_c and as such is probably not a good indicator for bed mobility.

Erosion thresholds and rates for variable-porosity beds

In contrast to the high-porosity bed experiments where only Type II erosion was observed (Fig. 3), four additional erosion types were observed in the variable-porosity bed experiments. The consistent sequence of occurrence of the erosion types during the experiment illustrates continuous evolution of bed erosion with increasing applied shear stress τ_0. However, considering the generally uniform properties of the material making up the bed, the occurrence of transitional Type I/II erosion indicates stratification of the bed erodibility. The maximum depth of erosion during transitional erosion is very shallow, extending to less than 0.2 mm. This indicates a transitional zone between the remoulded bed of uniform erodibility and the surface layer, which may reflect the disturbance of the bed at the sediment-water interface during the process of smoothening or during filling of the flume with water (see the bed preparation process in ”Methods and materials” under “Variable-porosity bed mobility”). Furthermore, erosion may cease at a given τ_0 and affect only the topmost part of the bed, thus displaying Type I erosion, if the velocity steps were extended by extra 10 to 30 min. In this case, the threshold at which constant erosion would take place (signifying the onset of erosion of a uniform erodibility bed) would be the Type II erosion threshold τ_c. Therefore, τ_c can be defined based on the onset of Type II erosion (Fig. 14).

A few studies on the mobility of calcareous nannofossil oozes have been conducted (Black et al., 2003; Southard et al., 1971). Additionally, work on shallow-water aragonitic lime mud provides insight on flocculation and bedload transport in fine-grained carbonate sediment (Schieber et al., 2013). Though mineralogically and texturally different, we may draw parallels between these experiments and the physical behaviour of chalk ooze. Erosion thresholds τ_c, based on the onset of Type II erosion, show a negative correlation with bed porosity φ. A similar relationship (Fig. 14) is also indicated in Southard et al. (1971) and

Black et al. (2003). Erosion threshold τ_c values from our study are slightly higher than the results of the two aforementioned studies suggesting a lower mobility of the chalk ooze compared to the heterogeneous modern pelagic ooze. The cause for generally lower τ_c values in Southard et al. (1971) might be due to differences in the threshold estimation process. Southard et al. (1971) estimated the onset of erosion as the point at which the first signs of particle motion were observed. Thus, it is possible that this method accounts for surface erosion only. Similar Type Is/IIs surface τ_c values to those of Southard et al. (1971) seems to confirm this assumption (Fig. 6) and indicate overestimation of ooze erodibility. Black et al. (2003) gives erosion threshold τ_c values as a range for the onset of Type I erosion. If the τ_c values from Black et al. (2003) are instead interpreted as the onset of constant Type II erosion (Fig. 14), these values are slightly higher compared to our data. However, a simple comparison between these studies considering the bed porosity φ as the main variable can be erroneous as heterogeneous grain size, variable content of clay, organic matter and siliceous sponge spicules may equally affect the mobility of the sediment. Nevertheless, comparison of modern ooze with almost pure chalk ooze of the same porosity yields comparable values in terms of erosion threshold τ_c suggesting an insignificant influence of these additional variables on chalk ooze mobility for the given range. Considering that clay minerals or organic matter would potentially increase the sediment cohesiveness and ultimately affect mobility (*e.g.* Mitchener and Torfs, 1996; Tolhurst et al., 2002). The erodibility of chalk ooze is generally much higher than that of cohesive siliciclastic mud with comparable porosities. For example, cohesive North Pacific red clay with similar bed porosities have τ_c ranging from 0.17–1.94 Pa (Lonsdale and Southard, 1974), and estuarine and intertidal mud of variable bed porosity φ and clay/organic matter content have τ_c between 0.19–2.0 Pa (Amos et al., 1996; Andersen, 2001). This marked difference in erodibility generally reflects the dominating clay fraction that, being the most electrochemically active sediment portion, in pelagic muds along with organic components (*e.g.* extracellular polymeric substances) in estuarine and intertidal muds drastically reduces cohesive siliciclastic mud mobility.

Of particular interest in our study is the development of exponential Type III erosion that to our knowledge has not been described in the sediment dynamics literature. Our observations show that Type III erosion occurs at bed shear stress τ_0 values exceeding 0.13 Pa in less consolidated beds with total porosity of 77.7 % (ρ_b = 1400 kg/m^3) and above bed τ_0 of 0.22 Pa in more consolidated (φ = 59.9 %; ρ_b = 1700 kg/m^3) beds.

This erosion type consistently follows a period of Type II erosion normally considered in the sediment dynamics literature as the final stage of erosion occurring only at the highest applied shear stresses (Amos et al., 1997; Tolhurst et al., 2009). The exact reason for the occurrence of this new erosion type is unknown because any visual observations were impaired due to high amount of suspended particles in the water column. One possible reason might be the failure of the bed due to a decrease in viscosity under application of certain τ_0, thus suggesting that chalk ooze displays either shear-thinning or time-dependant thixotropic properties. Alternatively, this could be caused by the entrainment of large bed aggregates travelling as bedload causing extensive erosion through a solid transmitted stress.

Unlithified nannofossil ooze at the sea bottom will undergo gradual lithification with time and increasing burial to form chalk (Scholle, 1977) with porosity values in the North Sea ranging from nearly 50 % to less than 5 % (Fabricius, 2007; Mallon and Swarbrick, 2002). Our experiments cover the porosity range of chalk ooze from 85 % to 60 % and may represent mobility of ooze that is buried up to 300 m, such as pelagic carbonate ooze on the Ontong Java Plateau (burial 0–293 m) with porosity values from 75–60 % (Fabricius and Borre, 2007). As our experiments exclude potential cementation that may occur with burial, sediment mobility with increasing burial depth may be overestimated. This factor can significantly influence chalk ooze mobility as seen from one experiment that may have experienced local cementation (experiment LC #8; Table 2) resulting in a ~13% higher erosion threshold τ_c and a 4 times lower erosion rate E_m at the same applied bed shear stress τ_0.

Deposition thresholds and still water deposition

Deposition thresholds τ_{cd} over a smooth flume floor without a sediment bed varied between 0.06 Pa and 0.08 Pa from suspensions of 0.9 and 1.7 g/l respectively (Fig. 9). This variability generally illustrates that faster-settling larger particles originated from higher initial suspension concentration and may suggest aggregation and flocculation of chalk ooze particles. In this scenario, larger aggregates would form in higher SSC's as a result of a higher chance of inter-particle collisions. Floccule size may vary with shear stress τ_0 and SSC as illustrated by Manning et al. (2007) in estuarine mud. However, in experiments with an underlying sediment bed, the deposition threshold τ_{cd} values do not relate to variability in SSC. In fact, a high variability of τ_{cd}

occurs at similar maximum suspended sediment concentration SSC_{max} values (Fig. 15 A). In these sets of experiments the material was brought into suspension by erosion of pre-existing beds (with various porosities) in the flume. The deposition phase of the experiment was initiated after reaching the SSC_{max} (1.4–1.8 g/l) at the maximum shear stress τ_{0max} during the erosion phase. The maximum shear stress τ_{0max} depends on the erodibility of the bed and correlates with the bed porosity φ (Table 4). Figure 15 B illustrates a linear relationship between τ_{cd} and maximum applied erosional shear stress τ_{0max}. The positive correlation suggests that τ_{0max} will control the τ_{cd} under conditions with similar SSC_{max} values. This relation most likely reflects the primary particle flocculation enhanced by shear. Higher τ_{0max} would enhance the particle flocculation, but never reach the τ_0 levels under which the floc disruption might occur. For example, Manning et al. (2007) observed floc disruption at τ_0 above 0.36 Pa that is significantly lower than τ_{0max} in the current study. However, the highest τ_{cd} values in experiments with a sediment bed are significantly higher than τ_{cd} in experiment without a sediment bed (see grey-coloured data points in Fig. 15 A, B), even though τ_{0max} and SSC_{max} values were higher in the latter experiment (run LC#12). This suggests that the positive correlation between τ_{cd} and τ_{0max} is due to other factors than SSC and the erosional shear stress τ_{0max} itself. The relation between bed porosity φ of the pre-depositional eroded bed and τ_{cd} (Fig. 15 C) is similar to that of τ_{0max} and τ_{cd} (Fig. 15 B). This implies a connection between the τ_{cd} and the properties of the bed from which the particles were eroded prior to deposition. Thus, the erosion of low-porosity beds took place at relatively high erosional shear stresses (τ_{0max}), probably by removal of relatively large aggregates which subsequently fell out of suspension at relatively high current velocities (high τ_{cd}). Conversely, high-porosity beds were eroded at low τ_{0max} and produced small particles which were deposited at low τ_{cd}. In addition, the deposition threshold τ_{cd} of particles produced from high-porosity beds may overlap with erosion thresholds τ_c. This is suggested by the fact data points representing porosities above 80 % appear to form a higher sloping trend than data points representing lower porosities (Fig. 15 C). Deposition thresholds τ_{cd} above high-porosity beds > 82 % (ρ_b < 1325 kg/m^3) are therefore much lower than above a smooth flume floor (Fig. 15 C), reflecting the high mobility and low erosion threshold τ_c values of ooze above beds with these porosities. This probably reflects that deposition occurring above the τ_c is overprinted by constant (Type II) erosion and net deposition would be registered by OBS only when shear stress τ_0 values are below the erosion threshold τ_c.

Consequently, this implies that when considering deposition from a moving current the interaction with the underlying sediment bed during the erosion phase and deposition phase needs to be considered. Most of our experiments show a deposition threshold τ_{cd} that exceeds the surface τ_c, which is commonly observed in siliciclastic cohesive sediments (*e.g.* Sanford and Halka, 1993).

Our experiments reveal a notable discrepancy between the calculated settling particle size and measured primary particle size. Thus the size of the settling particles estimated from W_s is 19–37 μm (Table 4), the grain size of suspended particles measured by laser diffraction is 6–16 μm (Fig. 12), whereas the mean size of the primary particles forming the ooze is 5–6 μm (Table 1). A possible reason could be inaccuracies in the calculation of particle size using the equation of Gibbs et al. (1971) that is used for settling velocity calculation of spheres. Another potential source of error may stem from the inaccuracy in estimating primary particle size using a particle laser-sizer due to the non-spherical nature of the nannofossil ooze forming grains (Buls et al., 2015). However, considering that the particle laser-sizer would most likely overestimate the volume and therefore also the mean grain size of non-spherical grains (Xu and Di Guida, 2003), the difference between the calculated size of settling particles and primary particles would still persist. Another explanation for this observed difference might be the flocculation and aggregation of primary particles forming larger aggregates that possess equivalent mass settling velocity W_s to its particle size. The flocculation of chalk ooze has not previously been reported. However, recent studies by Schieber et al. (2013) show flocculation of lime mud that, although different in terms of grain shape (needles) and mineralogy (aragonite, high-Mg calcite), illustrates that carbonate minerals may form floccules of comparable strength to those formed by clay minerals. Therefore, flocculation and aggregation of nannofossil ooze consisting almost entirely of low-Mg calcite seems possible. In fact, as the equivalent grain size was calculated for particles using calcite density 2710 kg/m^3, the actual aggregated and flocculated particle size might be much larger as the floccule density is highly variable and would be lower than the given calcite grain density.

Variations in the initial mass settling velocities W_s seen during the rapid settling phase (first 10 min, Fig. 11 A) might be caused by a high degree of variation of the shapes of the largest particles. However, it also appears that higher W_s occur for material that had a higher starting concentration during the mixing phase of

the experiment. This may be due to closer grain-grain proximities in higher initial SSCs promoting a higher degree of flocculation and aggregation of particles under equivalent applied shear stresses τ_0.

Suspended grain size variation

Classically, chalk ooze is viewed as sediment with little or no cohesion due to the lack of imbalanced inter-particle electric charges, particle interlocking or appreciable amounts of clay (Bramwell et al., 1999; Damholt and Surlyk, 2004; Nielsen et al., 1990). In terrigenous silts, the size fraction 2–10 μm is considered cohesive whereas the fraction 10–63 μm is sortable. By analogy, generally cohesive behaviour of nannofossil sediment might be expected in the size fraction 2–10 μm. This would exclude preferential particle removal in our study due to the low volume of particles larger than 10 μm (Table 1). Experimental studies by Black et al. (2003) illustrated winnowing at the bed surface under applied shear stress τ_0, where increasing stress entrains progressively larger particles such as tests of planktonic and benthic foraminifera. They observed progressive coarsening of resuspended particle/aggregate material from ~5–15 μm at applied $\tau_0 < 0.02$ Pa to 275–375 μm at 0.33 Pa. Furthermore, Cooke et al. (2004) interpreted current winnowing of fine-grained pelagic carbonate oozes in Neogene sediments on the Challenger Plateau, showing preferential removal of the 3–13 μm fraction and suggesting a non-cohesive nature of the fraction < 10 μm. Black et al. (2003) used heterogeneous calcareous ooze in their experiments, making comparison to the winnowing behaviour of much finer-grained, more homogeneous chalk ooze less than straightforward. Considering that indications of particle aggregation and flocculation have been observed in our experiments and that flocculation in lime mud is also described by Schieber et al. (2013), the question of chalk ooze cohesiveness is still unclear. Grabowski et al. (2011) noted that inter-particle attraction is the defining characteristic of cohesive sediment, describing cohesion as attraction between chemically similar particles or substances and distinguishing between aggregation of particles by cohesion (termed coagulation) and adhesion of dissimilar particles and substances (termed flocculation). This definition suggests that chalk ooze may be considered cohesive if coagulation of similarly sized chalk ooze particles occurs. Therefore, aggregation of primary chalk ooze particles into larger aggregates, as indicated by differences in size of the settling particles (Table 4), indicates cohesive behaviour. Also, the presence of a significant amount (up to 29 vol %) of particles < 2 μm (Table 1)

may contribute to increased cohesiveness of this already very fine-grained sediment. Additional experiments specifically designed to study these processes are necessary to confirm the coagulation and flocculation behaviour of chalk ooze. Even though the finer-grained part of the chalk ooze may be considered cohesive due to its aggregational behaviour or similarity in erosional behaviour to cohesive mud (i.e. development of different erosion types), the cohesion of chalk ooze is comparatively lower than that of pure siliciclastic muds as inferred from its generally higher mobility.

Variations in suspended primary particle sizes were observed during the erosion and deposition phases of the experiments using high-porosity beds after 24 h consolidation. These variations reflect the changes in primary particle size with the increasing erosion depth (Fig. 12 B) and shear stress τ_0 (Fig. 12 C). The suspended primary particle size decreases (Fig 13 B) close to the average grain size of the bed (Table 1) towards the end of the erosion phase, and increases during the deposition phase (Fig. 12 A). The grain-size variability with depth is expected to reflect the primary-particle composition in the top mm of the bed. This, however, contradicts what might be expected, as the bed is created by resuspension–settling to remove coarse-grained, non-disaggregated sub-1 mm fraction by differential settling (see Materials and Methods) and therefore should more likely form a normally-graded bed. If this mean grain-size decrease indeed reflects the actual primary particle composition at the top < 0.5 mm, what might be the possible explanation for the slight (mean grain size is between 6 and16 μm) coarsening upwards? Observations during deposition under applied shear stress τ_0 suggest a variation in particle size during this experimental phase (Fig. 12 A): floccules can be formed of unsorted and variously sized grains, but the smaller particles will flocculate more rapidly. Larger grains may not form flocs but can adhere to the flocs formed of fine particles (Kranck, 1973). If the suspended sediment concentration and applied τ_0 cease to promote any further flocculation, a scenario is plausible where initial flocculation of the smallest particles forms larger aggregates that settle faster than those individual particles that are larger than the particles forming floccules. This may form a relatively "coarser" grained upper part of the bed during settling that subsequently would be eroded first during the erosion phase of the following replication runs.

However, studies by Buls et al. (2015) did not observe signs of grading and changes in mean grain-size in the top 3 cm of the bed after the resuspension-settling. Therefore, if the bed is homogeneous and presumably

consists of coarser primary particles and aggregated or flocculated particles (formed of finer primary particles) with similar W_s, other processes must be responsible for variability in suspended grain-size during erosion of a homogeneous bed. Hypothetically, selective sorting can occur in very fine-grained chalk ooze with a limited grain size range under low applied shear stress τ_0, based on indications of particle aggregation and flocculation in the present study. As smaller particles have larger relative surface area and proportionally greater adhesive force than larger particles (Kranck, 1973) it is possible that at low τ_0, floccules composed of very small primary particles at the bed surface hypothetically could resist resuspension for longer compared with floccules composed of slightly larger grains that would break apart due to weaker particle–particle bonds. Therefore, with increasing shear stress τ_0, progressively finer particles (Fig. 12 A, C) would be introduced in the water column until τ_0 values greater than 0.08 Pa, when the grain-size of material in suspension (Fig. 12 B) is nearly identical to that of the bed (Table 1), indicating indiscriminate erosion without sorting.

Sub-resuspension threshold sediment dynamics

Sediment transport experiments using beds with porosities of 84 % and 79 % (ρ_b of 1295 and 1385 kg/m^3, respectively) revealed that the formation of sedimentary features at current velocities below the resuspension threshold is limited to high-porosity (~84 %) beds only. Our observations indicate that transport of poorly consolidated sediment can occur at the bed surface without the material being entrained into suspension at shear stress τ_0 values < 0.034 Pa. Low relief sedimentary features may develop (Fig. 13) if given sufficient time and sufficient loose material. The formation of these features occurred at even the lowest applied current velocity values < 0.02 Pa (0.10–0.11 m/s). However, their prominence only increased when progressively more material was mobilised at the bed surface under higher applied shear stress τ_0. The migration speed of the sedimentary features seemed to be dependent on the available loose material at the uppermost part of the bed with smaller features migrating faster than larger ones at the same current velocity (*e.g.* Fig. 13 C and 13 F). The transport of the material along the bed surface occurred at velocity values below the resuspension threshold of 0.05 Pa with a featureless surface developing at bed τ_0 values > 0.034 Pa. No sediment entrainment in suspension was observed during experiments at values below 0.034 Pa, indicated by consistent SSC values throughout the experiment. Development of individual small separate clouds of sediment, indicating bursting processes, were observed entering the suspension phase at the highest applied τ_0 of this experiment (0.034 Pa). This may reflect either a higher potential for resuspension of the remobilised material or the effect of form drag due to development of bed relief.

As seen from the sediment transport experiment with a high-porosity bed, the mobility of sediment at suberosion current velocities is essentially limited by the amount of sediment that can be mobilised without resuspension. Over a lower porosity bed, a low volume of material will be eroded at velocities close to the resuspension threshold, possibly reflecting a difference in the porosity between a thin loose-sediment layer at the water-sediment surface and deeper-lying homogeneous bed. This essentially illustrates that a low-porosity chalk ooze bed is immobile after the loose surface layer is removed and subjected to near-erosion threshold current velocities for an extended period of time. Therefore, mobilisation of sufficient amounts of material to form similar sedimentary features as seen in the experiment with higher porosity beds and τ_0 below 0.034 Pa is unlikely, because a lower porosity bed will be more resistant to mobilization. This

excludes the occurrence of sub-resuspension threshold transport in beds with $\varphi < 79$ % ($\rho_b > 1385$ kg/m^3). In our study, the transport occurs as a slow mass flow and we do not observe transport of individual floccules. Although the formation of sedimentary features was observed, we avoid labelling them as "ripples". The term "bedload transport" in muddy sediments is not precise because dynamic and continuous exchange is not observed between mobile bed particles and suspended particles (Tolhurst et al., 2009). Therefore we identify the terms "surface creep" and "benthic load" as more suitable to describe the observed sediment transport below the resuspension threshold. Reports of traction structures in fine-grained mud have not been limited to observations in lab flumes. For example, Gambacorta et al. (2014) interpreted wavy lamination as current ripples formed by sea-bottom currents in pelagic Upper Cretaceous Cenomanian limestones. In contrast, detailed studies of Upper Cretaceous contourite chalk have failed to identify traction structures due to pervasive bioturbation or absence of traction transport during deposition of the chalk (Rasmussen and Surlyk, 2012). However, our results illustrate the potential for development of current-induced sedimentary features in chalk ooze, a phenomenon previously considered impossible due to its fine-grained nature (*e.g.* Rasmussen and Surlyk, 2012).

CONCLUSIONS

Our experimental flume studies extend the present-day knowledge of the physical behaviour of chalk ooze and provide data on: erosion thresholds τ_c, erosion rates E_m, deposition thresholds τ_{cd}, mass settling W_s and sub-resuspension threshold dynamics of this sediment. Moreover, our experiments addressed the behaviour of the sediment surface (porosity 83–85 %) and sub-surface ooze (porosity 60–82 %).

The following summarizes our results:

1. Surface erosion thresholds τ_c were 0.05–0.08 Pa, whereas Type II τ_c were 0.05–0.19 Pa and depended upon bed porosity φ (60–85 %).
2. Erosion rates E_m also depended upon bed porosity φ. Surface ooze with porosity > 80% displays low cohesion and is eroded at a constant rate from the onset of Type II erosion. Erosion rates E_m of lower porosity beds decrease with depth of erosion due to increasing compaction with burial depth.

3. A previously undescribed erosion type (Type III) was observed in our experiments that displayed exponential increase of suspended sediment at the same applied shear stress τ_0. The reasons behind the development of this erosion type are not clear, but may reflect shear-thinning or thixotropy.
4. The typical sequence of erosion types that occurred in experiments with porosities below 77 % was: surface erosion (Type Is or IIs), transitional (Type I/II), constant (Type II) and exponential (Type III) erosion.
5. Average E_m was highly variable for different porosity beds between 5.2 x 10^{-6} kg/m^2/s after the onset of surface erosion to 5.1 x 10^{-4} kg/m^2/s after the onset of exponential erosion.
6. Net deposition thresholds τ_{cd} varied between ~0.04 and ~0.13 Pa and showed dependency on maximum suspended sediment concentration SSC_{max} and applied shear stress τ_{0max}. Deposition thresholds τ_{cd} were also affected by the size of previously eroded aggregates transported in suspension and therefore the porosity of the bed from which these aggregates were eroded.
7. Chalk ooze demonstrates a potential for aggregation and flocculation. In deposition experiments, increasing aggregate size was observed with higher applied τ_0 and higher suspended sediment concentrations. The settling particle size exceeds the mean primary particle size of the chalk ooze, thus indicating potential aggregation/flocculation of particles.
8. Selective sorting of calcareous nannofossil ooze during erosion of high-porosity beds under low applied shear stresses might explain the observed variation in suspended primary particle size with erosion depth and shear stress τ_0.
9. Slow sediment creep occurs in loosely consolidated chalk ooze (porosity ~84 %) at τ_0 values below 0.034 Pa at a rate between 0.9 cm/h and 12 cm/h and formed low-relief sedimentary features resembling ripples. Surface creep and, ultimately, formation of any sedimentary features is unlikely to occur in lower porosity beds if loose surface material is not readily available. This is because higher bed stability would require higher shear stress τ_0 to initiate any sediment movement. As a result, any mobilised sediment would be entrained in suspension.

ACKNOWLEDGMENTS

The study was carried out as part of a project "Understanding Basin-Scale Depositional Processes for Improved Reservoir Quality Prediction within the Chalk of the Danish Central Graben" in collaboration between Centre for Cross-disciplinary Chalk Research (C3), University of Copenhagen and School of Ocean and Earth Science, University of Southampton generously funded by Maersk Oil. Our thanks to chief editor Dr. T.D. Frank, associate editor Prof. J.J.G. Reijmer, and reviewers, especially Dr. J.T. Eggenhuisen, for valuable comments. Dr. G.J. Gilleaudeau is thanked personally for reviewing an early manuscript version. We also would like to acknowledge Dr. J. Moreau for his help with ADV data processing.

REFERENCES

Amos, C.L., Bergamasco, A., Umgiesser, G., Cappucci, S., Cloutier, D., DeNat, L., Flindt, M., Bonardi, M. and Cristante, S. (2004) The stability of tidal flats in Venice Lagoon – The results of in-situ measurements using two benthic, annular flumes. *Journal of Marine Systems*, **51,** 211–241.

Amos, C.L., Brylinsky, M., Sutherland, T.F., O'Brien, D., Lee, S. and Cramp, A. (1998) The stability of a mudflat in the Humber estuary, South Yorkshire, UK. *Geological Society, London, Special Publications*, **139,** 25–43.

Amos, C.L., Daborn, G.R., Christian, H.A., Atkinson, A. and Robertson, A. (1992) In situ erosion measurements on fine-grained sediments from the Bay of Fundy. *Marine Geology*, **108,** 175–196.

Amos, C.L., Droppo, I.G., Gomez, E.A. and Murphy, T.P. (2003) The stability of a remediated bed in Hamilton Harbour, Lake Ontario, Canada. *Sedimentology*, **50,** 149–168.

Amos, C.L., Feeney, T., Sutherland, T.F. and Luternauer, J.L. (1997) The stability of fine-grained sediments from the Fraser River delta. *Estuarine Coastal and Shelf Science*, **45,** 507–524.

Amos, C.L., Sutherland, T.F., Cloutier, D. and Patterson, S. (2000) Corrasion of a remoulded cohesive bed by saltating littorinid shells. *Continental Shelf Research*, **20,** 1291–1315.

Amos, C.L., Sutherland, T.F. and Zevenhuizen, J. (1996) The stability of sublittoral, fine-grained sediments in a subarctic estuary. *Sedimentology*, **43,** 1–19.

Andersen, T.J. (2001) Seasonal variation in erodibility of two temperate, microtidal mudflats. *Estuarine Coastal and Shelf Science*, **53,** 1–12.

Anderskouv, K., Damholt, T. and Surlyk, F. (2007) Late Maastrichtian chalk mounds, Stevns Klint, Denmark–Combined physical and biogenic structures. *Sedimentary Geology*, **200,** 57–72.

Anderskouv, K. and Surlyk, F. (2011) Upper Cretaceous chalk facies and depositional history recorded in the Mona-1 core, Mona Ridge, Danish North Sea. *Geological Survey of Denmark and Greenland Bulletin*, **25,** 1–60.

Anderskouv, K. and Surlyk, F. (2012) The influence of depositional processes on the porosity of chalk. *Geological Society of London, Journal*, **169,** 311–325.

Back, S., Van Gent, H., Reuning, L., Grotsch, J., Niederau, J. and Kukla, P. (2011) 3D seismic geomorphology and sedimentology of the Chalk Group, southern Danish North Sea. *Journal of the Geological Society*, **168,** 393–405.

Black, K.S., Peppe, O.C. and Gust, G. (2003) Erodibility of pelagic carbonate ooze in the northeast Atlantic. *Journal of Experimental Marine Biology and Ecology*, **285,** 143–163.

Bramwell, N.P., Caillet, G., Meciani, L., Judge, N., Green, M. and Adam, P. (1999) Chalk exploration, the search for a subtle trap. In: *Petroleum geology of North-West Europe: Proceedings of the 5th Conference* (Eds A.J. Fleet and S.A.R. Boldy), pp. 911–938, Geological Society of London.

Bromley, R.G. and Ekdale, A.A. (1987) Mass transport in European Cretaceous chalk–fabric criteria for its recognition. *Sedimentology*, **34,** 1079–1092.

Buls, T., Anderskouv, K., Fabricius, I.L., Friend, P.L., Thompson, C.E.L. and Stemmerik, L. (2015) Production of Calcareous Nannofossil Ooze For Sedimentological Experiments. *Journal of Sedimentary Research*, **85,** 1228–1237.

Burdige, D.J. (2006) *Geochemistry of marine sediments*. Princeton University Press Princeton.

Campbell, S.J.D. and Gravdal, N. (1995) The prediction of high porosity chalks in the East Hod Field. *Petroleum Geoscience*, **1,** 57–69.

Cloutier, D., Amos, C.L., Hill, P.R. and Lee, K. (2002) Oil erosion in an annular flume by seawater of varying turbidities: A critical bed shear stress approach. *Spill Science & Technology Bulletin*, **8,** 83–93.

Cloutier, D., LeCouturier, M.N., Amos, C.L. and Hill, P.R. (2006) The effects of suspended sediment concentration on turbulence in an annular flume. *Aquatic Ecology*, **40,** 555–565.

Cooke, P.J., Nelson, C.S., Crundwell, M.P., Field, B.D., Elkington, E.S. and Stone, H.H. (2004) Textural variations in Neogene pelagic carbonate ooze at DSDP Site 593, southern Tasman Sea, and their paleoceanographic implications. *New Zealand Journal of Geology and Geophysics*, **47,** 787–807.

Damholt, T. and Surlyk, F. (2004) Laminated–bioturbated cycles in Maastrichtian chalk of the North Sea: oxygenation fluctuations within the Milankovitch frequency band. *Sedimentology*, **51,** 1323–1342.

Esmerode, E.V., Lykke-Andersen, H. and Surlyk, F. (2007) Ridge and valley systems in the Upper Cretaceous chalk of the Danish Basin: contourites in an epeiric sea. In: *Economic and Palaeoceanographic Significance of Contourite Deposits* (Eds A.R. Viana and M. Rebesco), **276**, pp. 265–282, Geological Society of London, Special Publication 276.

Esmerode, E.V., Lykke-Andersen, H. and Surlyk, F. (2008) Interaction between bottom currents and slope failure in the Late Cretaceous of the southern Danish Central Graben, North Sea. *Geological Society of London, Journal*, **165,** 55–72.

Esmerode, E.V. and Surlyk, F. (2009) Origin of channel systems in the Upper Cretaceous Chalk Group of the Paris Basin. *Marine and Petroleum Geology*, **26,** 1338–1349.

Fabricius, I.L. (2007) Chalk: composition, diagenesis and physical properties. *Geological Society of Denmark, Bulletin*, **55,** 97–128.

Fabricius, I.L. and Borre, M.K. (2007) Stylolites, porosity, depositional texture, and silicates in chalk facies sediments. Ontong Java Plateau – Gorm and Tyra fields, North Sea. *Sedimentology*, **54,** 183–205.

Gale, A., Anderskouv, K., Surlyk, F. and Whalley, J. (2015) Slope failure of chalk channel margins: implications of an Upper Cretaceous mass transport complex, southern England. *Journal of the Geological Society*, **172,** 763–776.

Gale, A.S., Surlyk, F. and Anderskouv, K. (2013) Channelling versus inversion: origin of condensed Upper Cretaceous chalks, eastern Isle of Wight, UK. *Journal of the Geological Society*, **170,** 281–290.

Gambacorta, G., Bersezio, R. and Erba, E. (2014) Sedimentation in the Tethyan pelagic realm during the Cenomanian: Monotonous settling or active redistribution? *Palaeogeography Palaeoclimatology Palaeoecology*, **409,** 301-319.

Gennaro, M. and Wonham, J.P. (2014) Channel development in the chalk of the Tor Formation, North Sea. In: *From Depositional Systems to Sedimentary Successions on the Norwegian Continental Margin*, pp. 551–586. John Wiley & Sons, Ltd.

Gibbs, R.J., Matthews, M.D. and Link, D.A. (1971) Relationship between sphere size and settling velocity. *Journal of Sedimentary Petrology*, **41,** 7–18.

Grabowski, R.C., Droppo, I.G. and Wharton, G. (2011) Erodibility of cohesive sediment: The importance of sediment properties. *Earth-Science Reviews*, **105,** 101–120.

Hancock, J.M. (1975) The petrology of the Chalk. *Proceedings of the Geologists' Association*, **86,** 499–535.

Hardman, R.F.P. (1982) Chalk Reservoirs of the North Sea. *Geological Society of Denmark, Bulletin*, **30,** 119–137.

Herrmann, S. and Thierstein, H.R. (2012) Cenozoic coccolith size changes–Evolutionary and/or ecological controls? *Palaeogeography, Palaeoclimatology, Palaeoecology*, **333,** 92–106.

Hjuler, M.L. and Fabricius, I.L. (2009) Engineering properties of chalk related to diagenetic variations of Upper Cretaceous onshore and offshore chalk in the North Sea area. *Journal of Petroleum Science and Engineering*, **68,** 151–170.

Honjo, S. (1976) Coccoliths: production, transportation and sedimentation. *Marine Micropaleontology*, **1,** 65–79.

Håkansson, E., Bromley, R. and Perch-Nielsen, K. (1974) Maastrichtian chalk of north-west Europe–a pelagic shelf sediment. In: *Pelagic Sediments on Land and Under the Sea* (Eds K.J. Hsü and H.C. Jenkyns), **1**, pp. 211–233. Blackwell Publishing Ltd., Oxford, UK.

Jarvis, I. (2006) The Santonian-Campanian phosphatic chalks of England and France. *Proceedings of the Geologists Association*, **117,** 219–237.

Kennedy, W.J. (1980) Aspects of chalk sedimentation in the southern Norwegian offshore. In: *Proceedings of the Symposium 'The sedimentation of the North Sea Reservoir Rocks', Geilo, 11–14 May, 1980, Paper 9*, pp. 1–29. Norwegian Petroleum Society, Stavanger.

Kennedy, W.J. (1987a) Late Cretaceous and Early Palaeocene Chalk Group sedimentation in the Greater Ekofisk area, North Sea Central Graben. *Bulletin des Centres de Recherches Exploration-Production Elf-Aquitaine*, **11,** 91–126.

Kennedy, W.J. (1987b) Sedimentology of Late Cretaceous–Palaeocene chalk reservoirs, North Sea Central Graben. In: *Petroleum Geology of North West Europe* (Eds J. Brooks and K. Glennie), pp. 469–481. Graham & Trotman, London.

Kim, S.C., Friedrichs, C.T., Maa, J.P.Y. and Wright, L.D. (2000) Estimating bottom stress in tidal boundary layer from Acoustic Doppler Velocimeter data. *Journal of Hydraulic Engineering*, **126,** 399–406.
Kontrovitz, M., Kilmartin, K.C. and Snyder, S.W. (1979) Threshold velocities of tests of planktic foraminifera. *Journal of Foraminiferal Research*, **9,** 228–232.
Kranck, K. (1973) Flocculation of Suspended Sediment in the Sea. *Nature*, **246,** 348–350.
Lefebvre, A., Thompson, C.E.L. and Amos, C.L. (2010) Influence of Zostera marina canopies on unidirectional flow, hydraulic roughness and sediment movement. *Continental Shelf Research*, **30,** 1783–1794.
Lonsdale, P. and Southard, J.B. (1974) Experimental Erosion of North Pacific Red Clay. *Marine Geology*, **17,** M51–M60.
Lykke-Andersen, H. and Surlyk, F. (2004) The Cretaceous–Palaeogene boundary at Stevns Klint, Denmark: inversion tectonics or sea-floor topography? *Geological Society of London, Journal*, **161,** 343–352.
Mallon, A.J. and Swarbrick, R.E. (2002) A compaction trend for non-reservoir North Sea Chalk. *Marine and Petroleum Geology*, **19,** 527–539.
Manning, A.J., Friend, P.L., Prowse, N. and Amos, C.L. (2007) Estuarine mud flocculation properties determined using an annular mini-flume and the LabSFLOC system. *Continental Shelf Research*, **27,** 1080–1095.
Mehta, A.J. and Partheniades, E. (1982) Resuspenion of deposited cohesive sediment beds. In: *Eighteenth Conf. Coastal Eng.*, pp. 1569–1588.
Mitchener, H. and Torfs, H. (1996) Erosion of mud/sand mixtures. *Coastal Engineering*, **29,** 1–25.
Neumann, A.C., Gebelein, C.D. and Scoffin, T.P. (1970) Composition, structure and erodability of subtidal mats, Abaco, Bahamas. *Journal of Sedimentary Petrology*, **40,** 274–297.
Nielsen, E.B., Fraselle, G. and Vianello, L. (1990) Tommeliten Gamma Field – Norway Central Graben, North Sea. In: *TR: Structural Traps IV: Tectonic and Nontectonic Fold Traps* (Eds E.A. Beaumont and N.H. Foster), pp. 85–112. AAPG Special Volumes.
Nygaard, E., Lieberkind, K. and Frykman, P. (1983) Sedimentology and reservoir parameters of the Chalk Group in the Danish Central Graben. *Geologie en Mijnbouw*, **62,** 177–190.
Oehmig, R. (1993) Entrainment of planktonic foraminifera: effect of bulk density. *Sedimentology*, **40,** 869–877.
Pope, N.D., Widdows, J. and Brinsley, M.D. (2006) Estimation of bed shear stress using the turbulent kinetic energy approach – A comparison of annular flume and field data. *Continental Shelf Research*, **26,** 959–970.
Prager, E.J., Southard, J.B. and VivoniGallart, E.R. (1996) Experiments on the entrainment threshold of well-sorted and poorly sorted carbonate sands. *Sedimentology*, **43,** 33–40.
Quine, M. and Bosence, D. (1991) Stratal geometries, facies and sea-floor erosion in Upper Cretaceous Chalk, Normandy, France. *Sedimentology*, **38,** 1113–1152.
Rasmussen, S.L. and Surlyk, F. (2012) Facies and ichnology of an Upper Cretaceous chalk contourite drift complex, eastern Denmark, and the validity of contourite facies models. *Journal of the Geological Society*, **169,** 435–447.
Sanford, L.P. and Halka, J.P. (1993) Assessing the paradigm of mutually exclusive erosion and deposition of mud, with examples from upper Chesapeake Bay. *Marine Geology*, **114,** 37–57.
Schieber, J., Southard, J.B., Kissling, P., Rossman, B. and Ginsburg, R. (2013) Experimental deposition of carbonate mud from moving suspensions: Importance of flocculation and implications for modern and ancient carbonate mud deposition. *Journal of Sedimentary Research*, **83,** 1025–1031.
Scholle, P.A. (1977) Chalk diagenesis and its relation to petroleum exploration: oil from chalks, a modern miracle? *American Association of Petroleum Geologists, Bulletin*, **61,** 982–1009.
Soulsby, R.L. (1983) The Bottom Boundary Layer of Shelf Seas. In: *Physical Oceanography of Coastal and Shelf Seas* (Ed B. Johns), pp. 189–266. Elsevier, Amsterdam.
Southard, J.B., Young, R.A. and Hollister, C.D. (1971) Experimental Erosion of Calcareous Ooze. *Journal of Geophysical Research*, **76,** 5903–5909.
Stapleton, K.R. and Huntley, D.A. (1995) Seabed stress determinations using the inertial dissipation method and the turbulent kinetic energy method. *Earth Surface Processes and Landforms*, **20,** 807–815.

Steinmetz, J.C. (1994) Sedimentation of coccolithophores. In: *Coccolithophores* (Eds A. Winter and W.G. Siesser), pp. 179–197. Cambridge University Press, Cambridge.

Surlyk, F., Dons, T., Clausen, C.K. and Higham, J. (2003) Upper Cretaceous. In: *The Millenium Atlas: Petroleum Geology of the Central and the North Sea* (Eds D. Evans, C. Graham, A. Armour and P. Bathurst), pp. 213–233. The Geological Society of London, London.

Surlyk, F., Jensen, S.K. and Engkilde, M. (2008) Deep channels in the Cenomanian–Danian Chalk Group of the German North Sea sector: Evidence of strong constructional and erosional bottom currents and effect on reservoir quality distribution. *American Association of Petroleum Geologists, Bulletin*, **92,** 1565–1586.

Surlyk, F. and Lykke-Andersen, H. (2007) Contourite drifts, moats and channels in the Upper Cretaceous chalk of the Danish Basin. *Sedimentology*, **54,** 405–422.

Surlyk, F., Rasmussen, S.L., Boussaha, M., Schioler, P., Schovsbo, N.H., Sheldon, E., Stemmerik, L. and Thibault, N. (2013) Upper Campanian–Maastrichtian holostratigraphy of the eastern Danish Basin. *Cretaceous Research*, **46,** 232–256.

Sutherland, T.F., Amos, C.L. and Grant, J. (1998) The erosion threshold of biotic sediments: a comparison of methods (Eds K.S. Black, D.M. Paterson and A. Cramp), **139**, pp. 295–307. Geological Society Special Publication.

Thompson, C.E.L., Amos, C.L., Angelaki, M., Jones, T.E.R. and Binks, C.E. (2006) An evaluation of bed shear stress under turbid flows. *Journal of Geophysical Research–Oceans*, **111**.

Thompson, C.E.L., Amos, C.L., Jones, T.E.R. and Chaplin, J. (2003) The manifestation of fluid-transmitted bed shear stress in a smooth annular flume – a comparison of methods. *Journal of Coastal Research*, **19,** 1094–1103.

Thompson, C.E.L., Amos, C.L., Lecouturier, M. and Jones, T.E.R. (2004) Flow deceleration as a method of determining drag coefficient over roughened flat beds. *Journal of Geophysical Research–Oceans*, **109**.

Thompson, C.E.L., Couceiro, F., Fones, G.R. and Amos, C.L. (2013) Shipboard measurements of sediment stability using a small annular flume-Core Mini Flume (CMF). *Limnology and Oceanography–Methods*, **11,** 604–615.

Thompson, C.E.L., Couceiro, F., Fones, G.R., Helsby, R., Amos, C.L., Black, K., Parker, E.R., Greenwood, N., Statham, P.J. and Kelly-Gerreyn, B.A. (2011) In situ flume measurements of resuspension in the North Sea. *Estuarine, Coastal and Shelf Science*, **94,** 77–88.

Tolhurst, T.J., Black, K.S. and Paterson, D.M. (2009) Muddy Sediment Erosion: Insights from Field Studies. *Journal of Hydraulic Engineering*, **135,** 73–87.

Tolhurst, T.J., Gust, G. and Paterson, D.M. (2002) The influence of an extracellular polymeric substance (EPS) on cohesive sediment stability. In: *Fine Sediment Dynamics in the Marine Environment* (Eds J.C. Winterwerp and C. Kranenburg), *Proceedings in Marine Science, v. 5*, **5**, pp. 409–425. Elsevier, Amsterdam.

van der Molen, A.S., van Heel, H.W.D. and Wong, T.E. (2005) The influence of tectonic regime on chalk deposition: examples of the sedimentary development and 3D-seismic stratigraphy of the Chalk Group in the Netherlands offshore area. *Basin Research*, **17,** 63–81.

Watts, N.L., Lapre, J.F., Vanschijndelgoester, F.S. and Ford, A. (1980) Upper Cretaceous and lower Tertiary chalks of the Albuskjell area, North-Sea: Deposition in a slope and a base-of-slope environment. *Geology*, **8,** 217–221.

Widdows, J., Friend, P.L., Bale, A.J., Brinsley, M.D., Pope, N.D. and Thompson, C.E.L. (2007) Inter-comparison between five devices for determining erodability of intertidal sediments. *Continental Shelf Research*, **27,** 1174–1189.

Xu, R.L. and Di Guida, O.A. (2003) Comparison of sizing small particles using different technologies. *Powder Technology*, **132,** 145–153.

Young, R.A. and Mann, R. (1985) Erosion velocities of skeletal carbonate sands, St. Thomas, Virgin Islands. *Marine Geology*, **69,** 171–185.

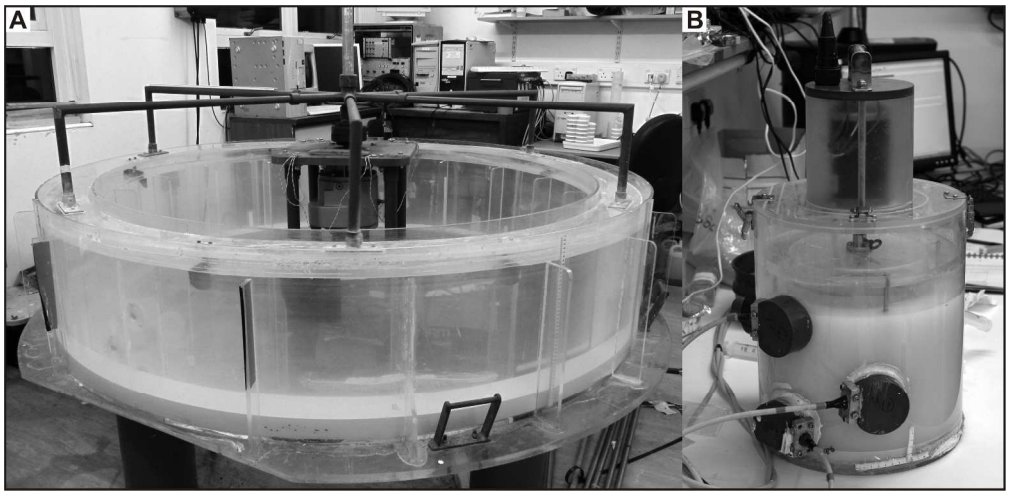

Fig. 1. Annular flumes used in experiments: (A) Lab Carousel and (B) Mini-Flume. Lab Carousel has a diameter of 2.0 m, with 0.15 m wide and 0.40 m deep channel. Mini-Flume has a diameter of 0.305 m, with 0.045 m wide channel and the maximum water depth used in the experiments of 0.22 m.

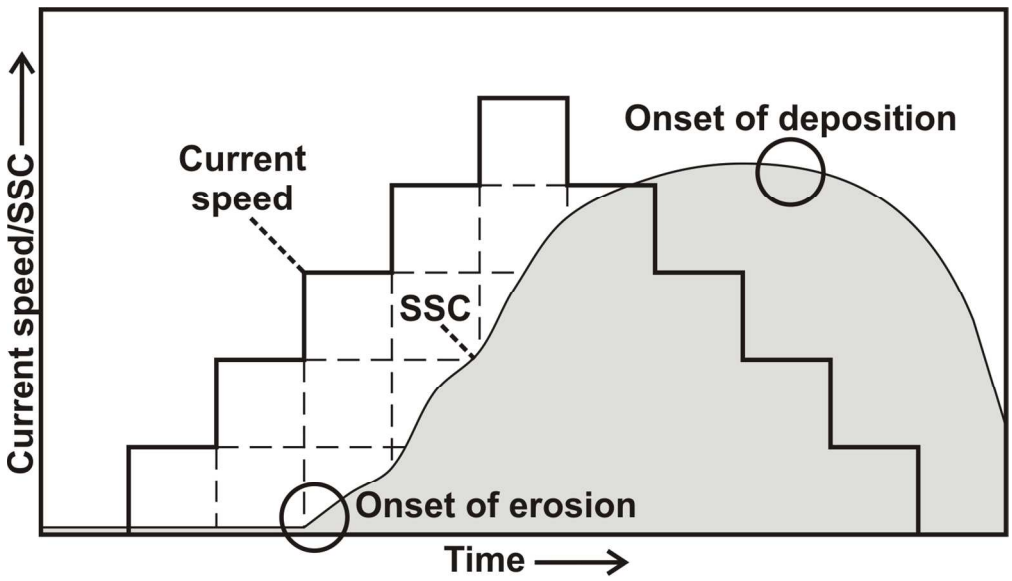

Fig. 2. General experiment design used to estimate erosion τ_c and deposition threshold τ_{cd}, erosion rates E_m and mass settling velocity W_s after the last velocity step.

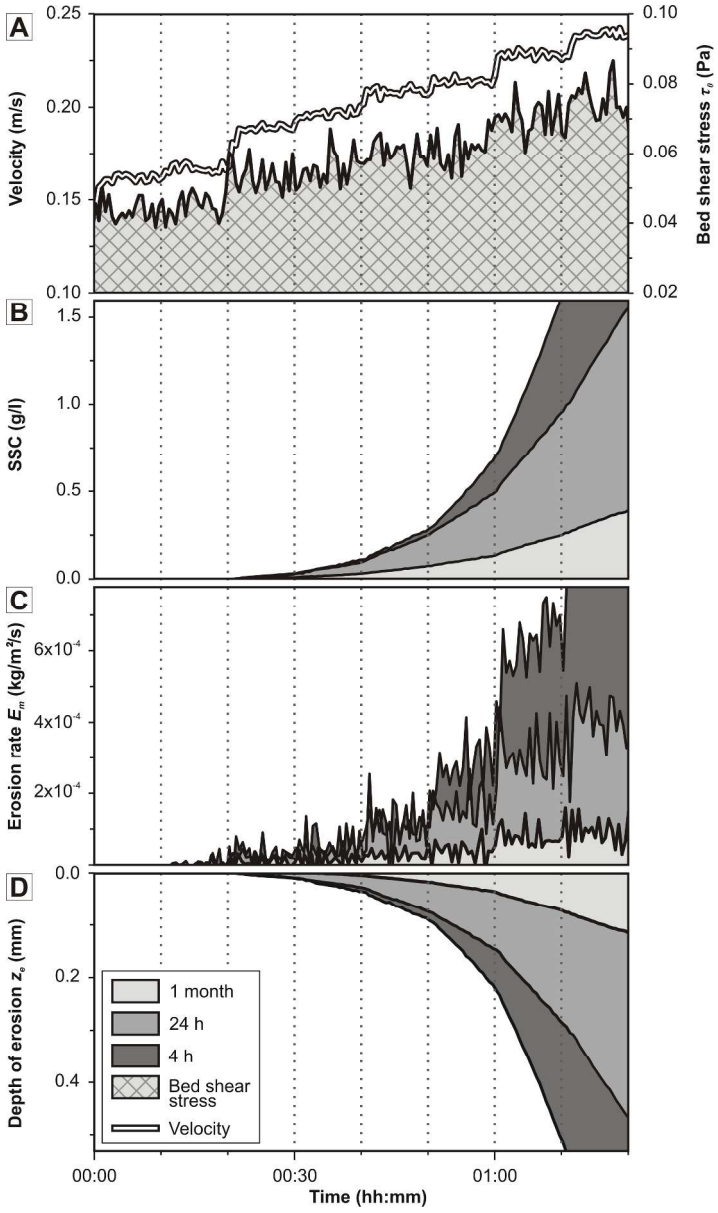

Fig. 3. Experiments studying mobility of surface ooze after bed consolidation of 4 h, 24 h and 1 month. Velocity and applied bed shear stress τ_0 (A), time series of (B) suspended sediment concentration (SSC), (C) erosion rate E_m and (D) depth of erosion z_e. Corresponding velocity steps (each 10 min) indicated with dotted vertical lines.

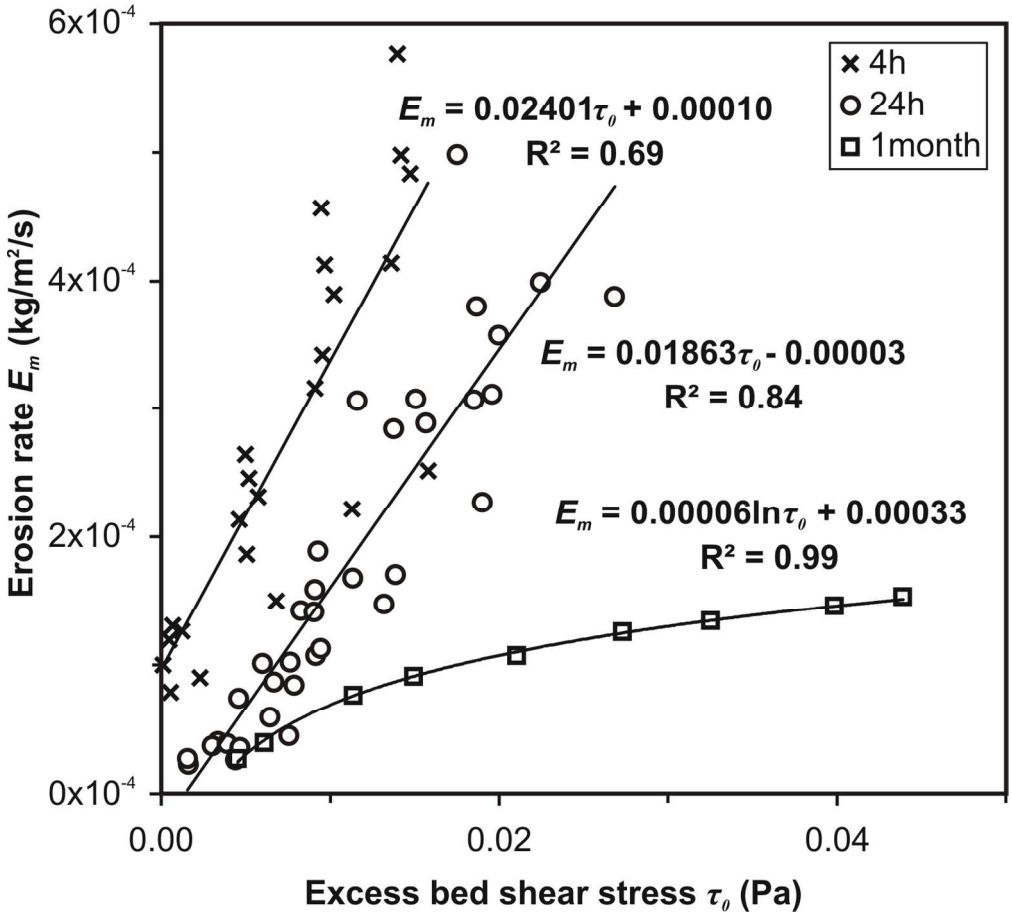

Fig. 4. Linear relationship between excess bed shear stress τ_0 and erosion rate E_m with the exception of the 1 month consolidation experiment that shows a logarithmic relation between excess τ_0 and E_m.

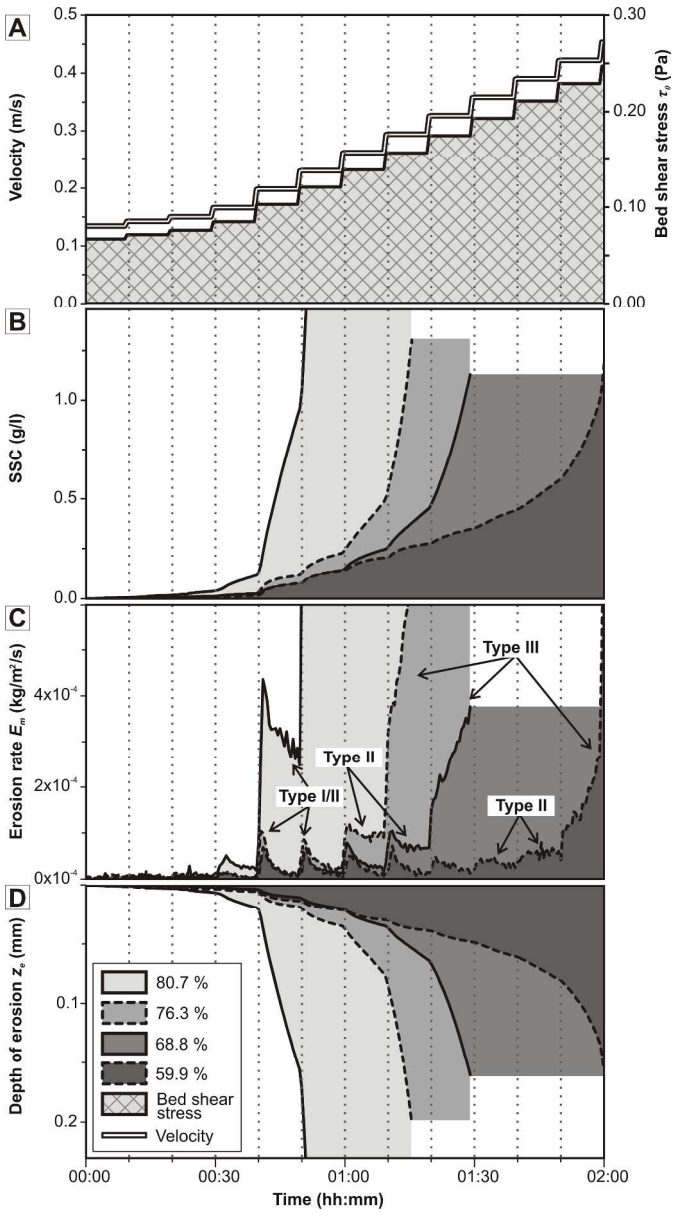

Fig. 5. Overview of variable-porosity bed experiments with bed porosities of 80.7 %, 76.3 %, 68.8 % and 59.9 %. Applied velocity and bed shear stress τ_0 (A), time-series of SSC (B), erosion rate E_m (C) and erosion depth z_e (D) illustrate development of different types of erosion with increasing applied τ_0. The first 45 min of experiment time that showed no development of erosion have been excluded.

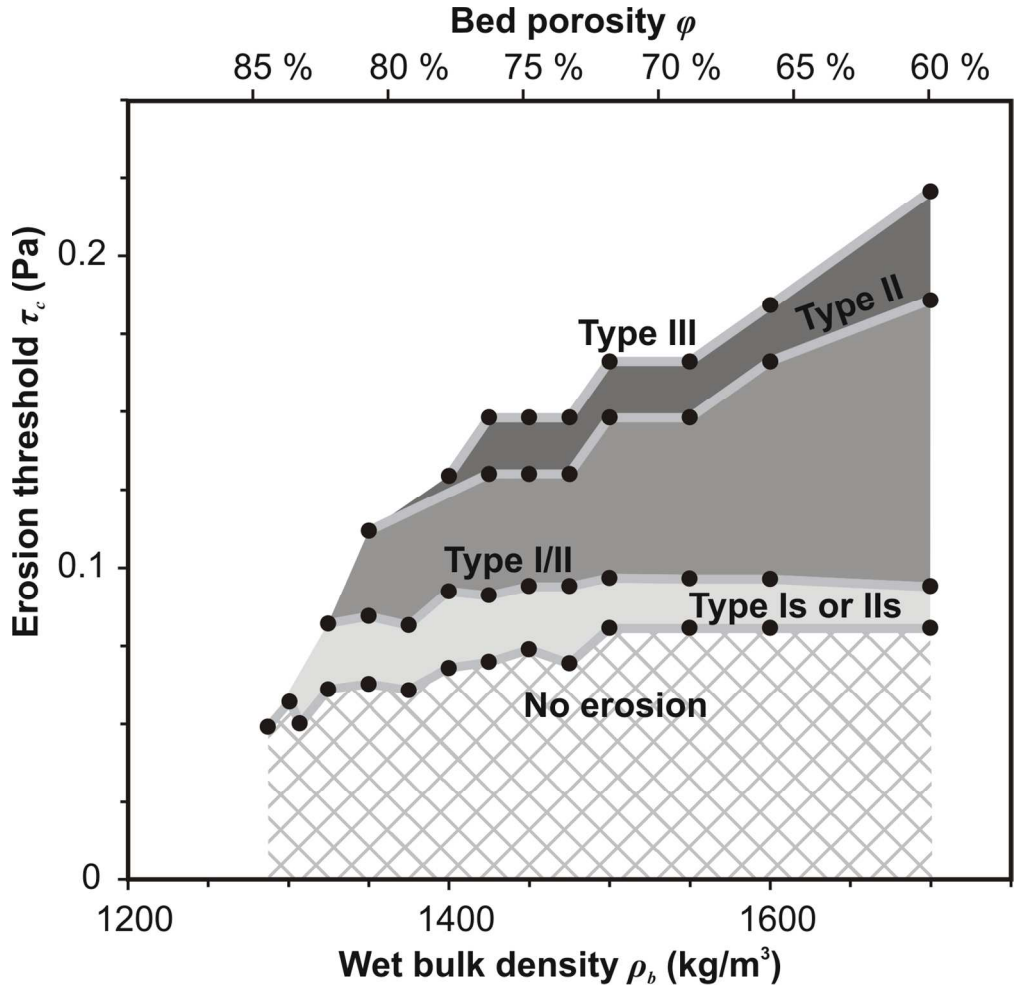

Fig. 6. Development of bed erosion with decreasing bed porosity φ and increasing shear stress τ_0. Summary of threshold τ_c values for occurrence of different types of erosion.

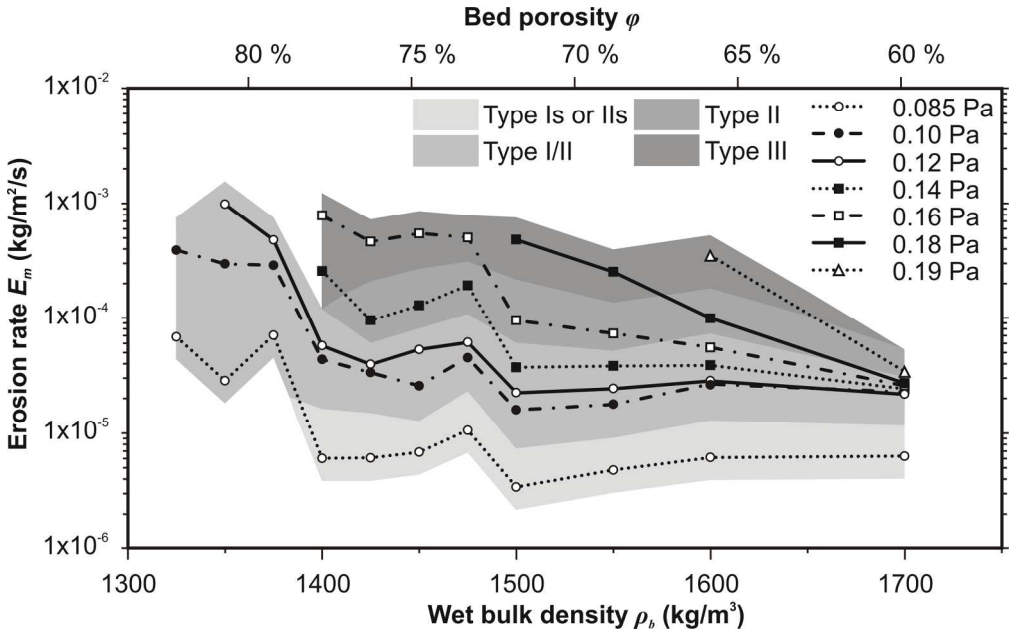

Fig. 7. Erosion intensity at given applied bed shear stress τ_0 observed for different chalk ooze bed porosities φ with shaded areas indicating the types of erosion.

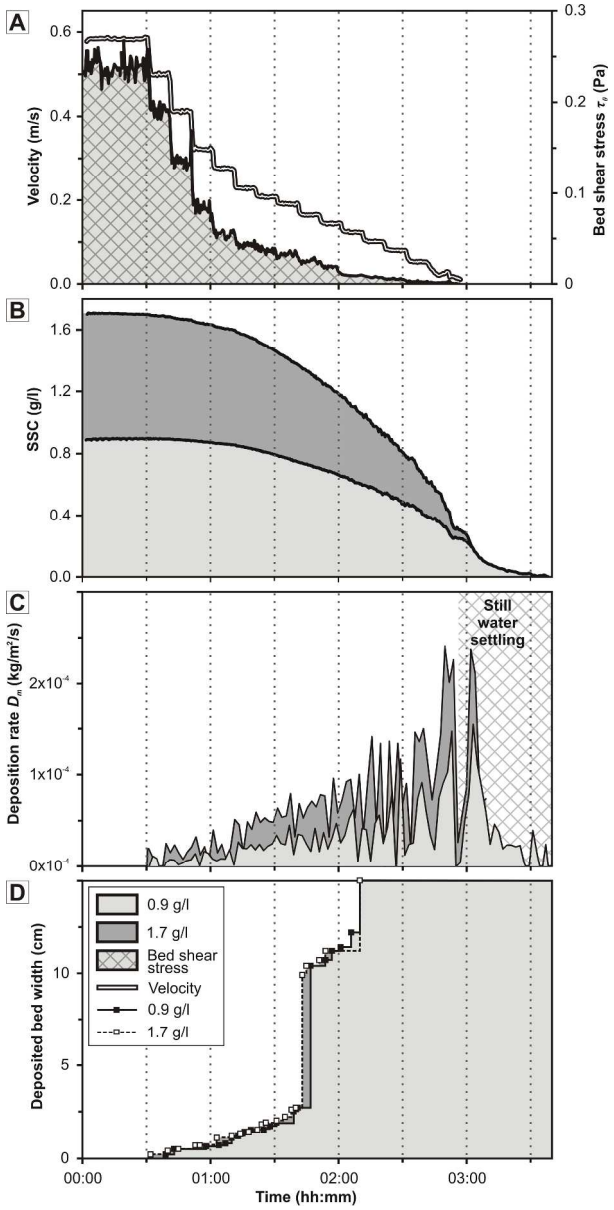

Fig. 8. Deposition under variable applied shear stress τ_0 on a smooth flume floor. Applied velocity and bed shear stress τ_0 (A); (B) time series of SSC of two experiments with initial suspended sediment concentration of 0.9 g/l and 1.7 g/l (runs LC #10 and LC #12 respectively); (C) deposition rates D_m; (D) observed deposition of the suspended material on the bed measured as sediment band from the inner side of the flume.

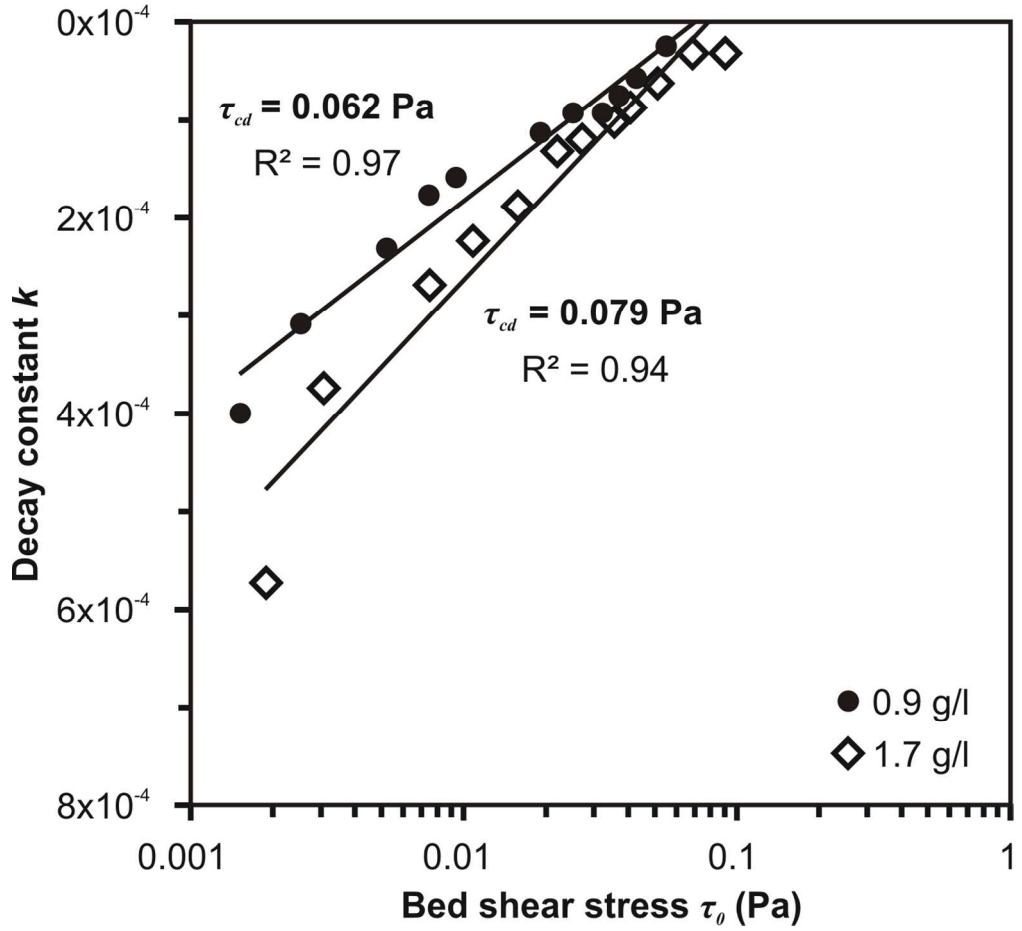

Fig. 9. Example of estimated depositional threshold τ_{cd} for material depositing from 0.9 g/l and 1.7 g/l suspension on a smooth flume floor. The settling under applied shear stress τ_0 followed an exponential decay law, under which the decay constant k is dependent on the applied τ_0. The depositional threshold τ_{cd} is found by regressing the k vs τ_0 (note the loglinear relationship) and solving for k=0 (Amos et al., 2004).

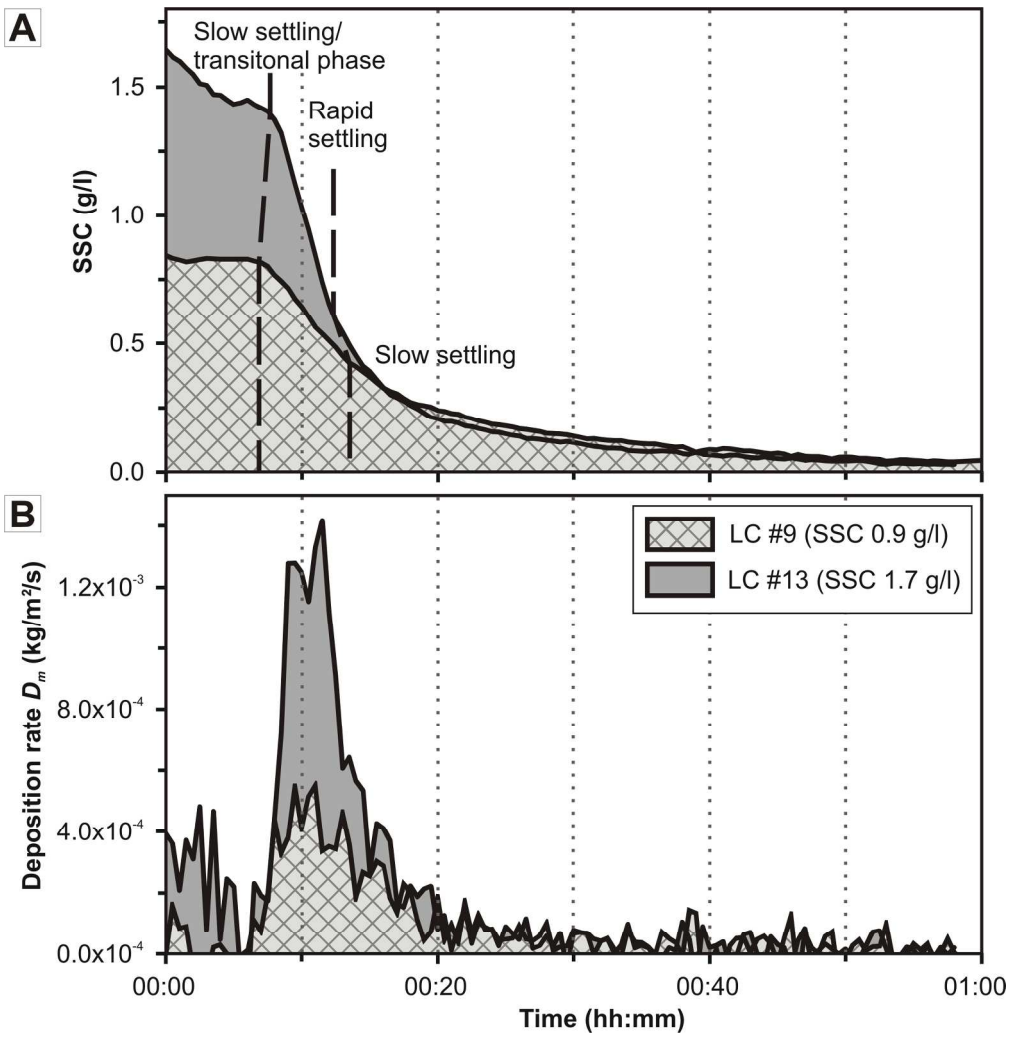

Fig. 10. Time series of SSC (A) and deposition rates D_m (B) from different starting concentrations during still-water phase directly after intensive mixing at velocity ~0.60 m/s (runs LC #9 and #13). Note that runs LC #9 and #10 had initial start concentration of 0.9 g/l and 1.7 g/l, respectively.

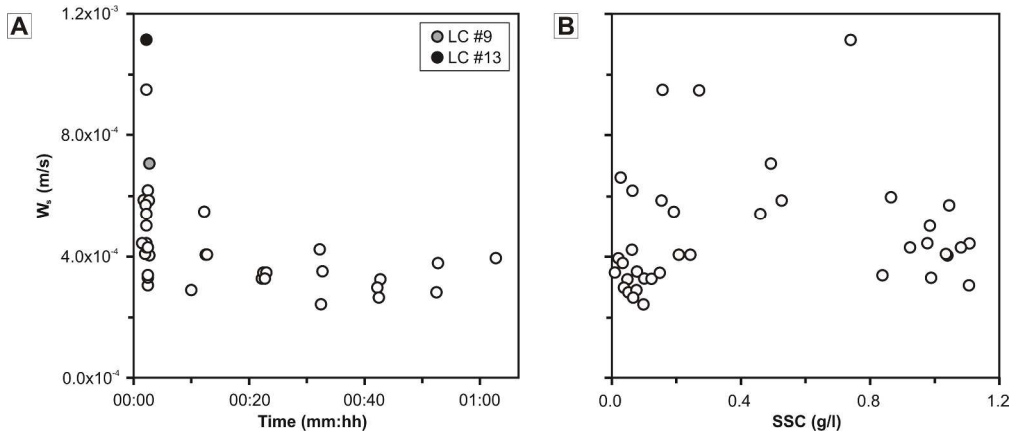

Fig. 11. Summary of mass settling velocity W_s data from all flume runs: (A) Variation in values of W_s with increasing settling time and decreasing suspended sediment concentration (SSC). Different colour data points indicate the average value over the first 10 min of experiments with different initial concentrations (see Fig. 10 for reference). (B) W_s values vs SSC, plotted are average values over 10 min intervals. No trends between SSC and W_s were observed.

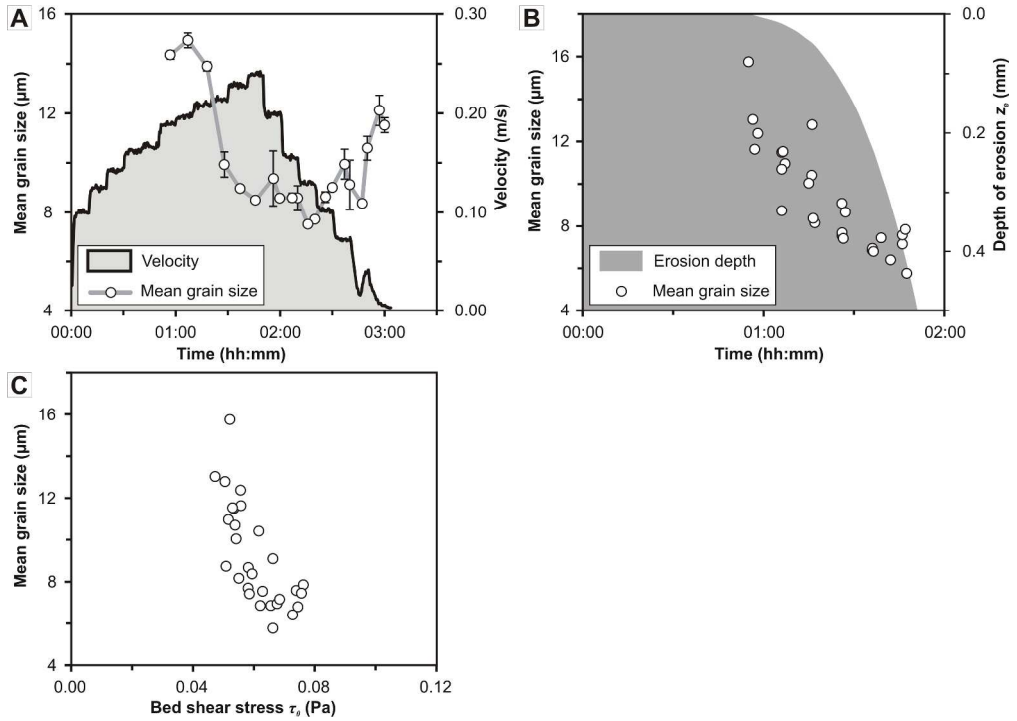

Fig. 12. Variation in measured suspended primary particle size during experiments using laser diffraction granulometer Coulter LS 130. (A) Time-series of experiment LC #6 (Table 2), show decrease and increase of suspended grain size with changing flow velocity. Summary of grain size variation over all 24 h consolidation experiments (B and C) show continuous decrease of suspended primary particle size after onset of erosion and increasing entrainment of eroded material into suspension following an increase in bed shear stress τ_0.

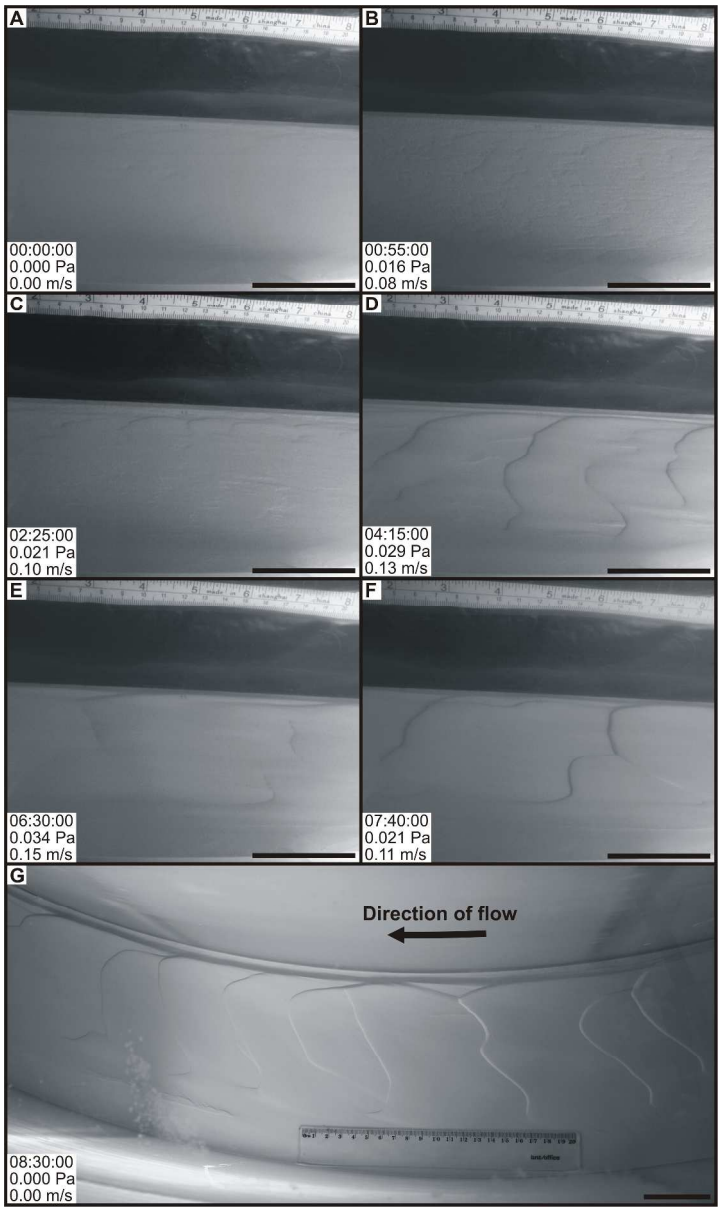

Fig. 13. Time-lapse of sub-resuspension threshold τ_c sediment transport experiment, pictures taken before (A), during (B–F) and at the end (G) of the experiment. Side-view (A–F) and top-view (G) of the bed (in all pictures direction of the flow is from right to left). Elapsed time after the start of the experiment, with corresponding measured current speed and bed shear stress τ_0 is indicated in each photograph, the scale-bar at the right side is 5 cm.

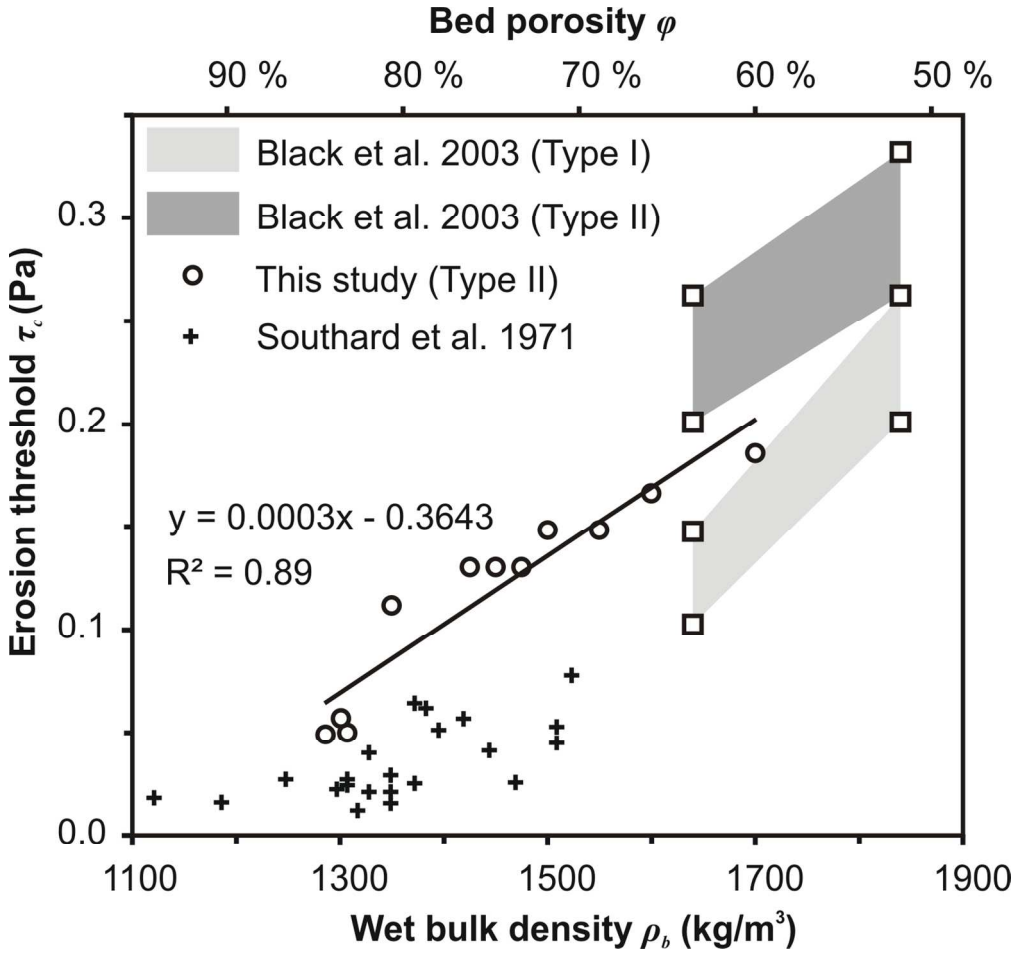

Fig. 14. Relation between the erosion threshold τ_c and bed porosity φ, and comparison with previously published work on pelagic nannofossil oozes by Southard et al. (1971) and Black et al. (2003). Erosion threshold τ_c for the onset of Type II erosion is displayed from our study. The shaded zone in Black et al. (2003) indicates range of τ_c for the onset of Type I and Type II erosion.

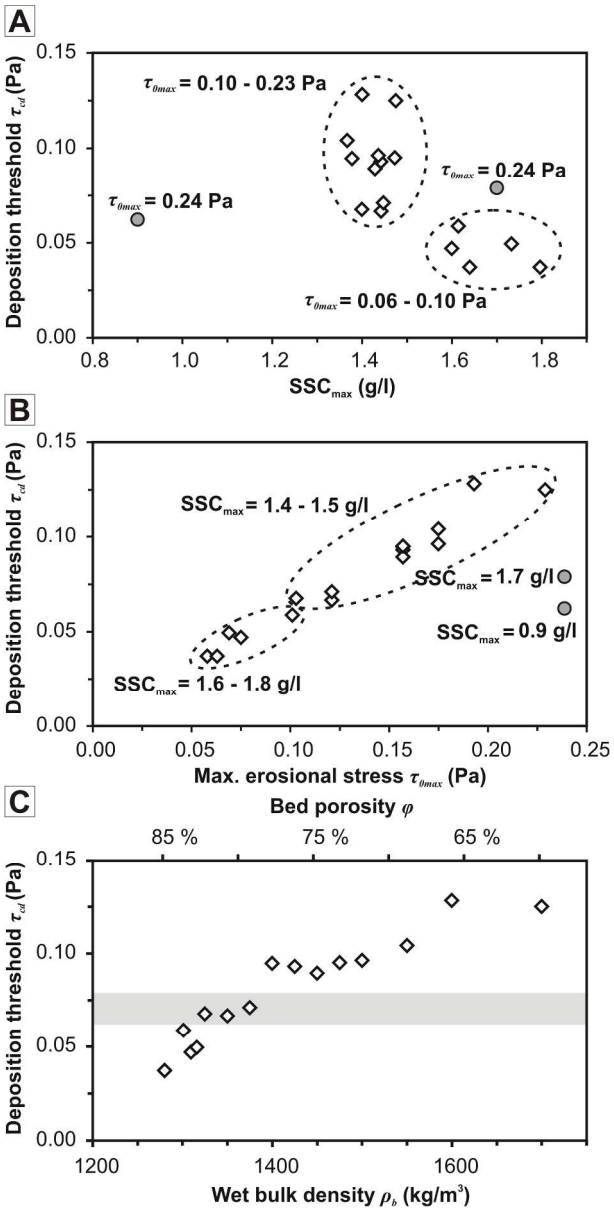

Fig. 15. Variability in deposition thresholds τ_{cd} in combined erosion–deposition experiments. (A) The estimated τ_{cd} plotted against the maximum suspended sediment concentration SSC_{max} at the maximum applied erosional shear stress τ_{0max}. τ_{0max} value is indicated next to the data points. (B) Relation between the τ_{cd} and τ_{0max}, with indicated SSC_{max} prior to start of deposition. Grey-coloured data points are from experiments on a smooth flume floor (see Fig. 8 for reference) illustrating the variability of deposition threshold τ_{cd} dependent only on SSC_{max}. (C) Relation between τ_{cd} and the initial bed porosity φ of the eroded bed from which the depositing particles were formed. Shaded zone indicates the range of τ_{cd} in experiments on a smooth flume floor.

Table 1. Measured grain-size and mineral composition of the sediment. The term "Original ooze" represents the disaggregated chalk ooze prior to employment in the flumes (Buls et al., 2015). "High-porosity ooze (Lab carousel)" represents ooze used in high-porosity bed experiments in Lab Carousel. "High-porosity ooze (Mini-flume)" represents ooze used in high-porosity bed experiments in Mini-flume (sieved through 212 µm mesh). "Variable-porosity ooze" represents ooze used in variable-porosity bed experiments in Mini-flume (sieved through 212 µm mesh).

	Grain size					
	D_{50}, µm	Mean, µm	> 20 µm	10-20 µm	< 10 µm	< 2 µm
Original ooze	5.9 ± 0.3	6.8 ± 1.2	11.9 ± 5.1 %	11.8 ± 1.0 %	76.3 ± 5.0 %	14.8 ± 1.0 %
High-porosity ooze (Lab carousel)	4.6 ± 0.6	5.6 ± 0.5	1.4 ± 1.3 %	10.4 ± 2.4 %	88.2 ± 2.3 %	25.7 ± 4.1 %
High-porosity ooze (Mini-flume)	4.1 ± 0.3	5.0 ± 0.3	0.7 ± 0.9 %	8.1 ± 1.2 %	91.2 ± 1.3 %	29.1 ± 2.5 %
Variable-porosity ooze	4.2 ± 0.4	5.4 ± 0.4	2.0 ± 1.1 %	8.1 ± 1.1 %	89.9 ± 1.5 %	27.7 ± 3.4 %
	Mineral composition, wt %					
$CaCO_3$	98.3-98.6					
SiO_2	0.46-0.56					
PO_4	0.11-0.14					
Feldspar	0.09-0.11					
Smectite	0.69-0.84					
Illite	0.05-0.06					

Table 2. Summary of experiments studying the mobility of high-porosity ooze settled from suspension and consolidated for 4h, 24h or 1 month, given total bed porosity φ and wet bulk density ρ_b values. "MF" and "LC" indicates experiments performed in "Mini-flume" and "Lab Carousel" accordingly with observed erosion thresholds τ_c. τ_{0max} indicates the maximum applied shear stress during the last step of experiment, E_m is the average erosion rate and z_e is the final erosion depth at τ_{0max}.

Run	Consolidation time	φ	ρ_b (kg/m^3)	τ_c (Pa)	E (kg/m^2/s)	r^2	z_e (mm)	Erosion type	τ_{0max} *(Pa)*	E_m (kg/m^2/s)
MF #1	4 hours	84.3%	1290	0.049	$E = 0.02319\tau_0 - 0.00010$	0.99	0.5	Type II	0.063	4.1×10^{-4}
MF #2	4 hours	83.2%	1308	0.051	$E = 0.01233\tau_0 - 0.00007$	0.98	0.4	Type II	0.067	2.5×10^{-4}
MF #3	4 hours	84.9%	1280	0.048	$E = 0.02921\tau_0 - 0.00005$	0.99	0.3	Type II	0.058	3.4×10^{-4}
MF #4	4 hours	84.9%	1280	0.048	$E = 0.02732\tau_0 - 0.00009$	0.99	0.5	Type II	0.063	4.8×10^{-4}
MF #5	4 hours	84.9%	1280	0.048	$E = 0.02820\tau_0 - 0.00011$	0.99	0.5	Type II	0.063	5.0×10^{-4}
MF #6	4 hours	84.9%	1280	0.049	$E = 0.03476\tau_0 - 0.00010$	0.99	0.5	Type II	0.063	5.8×10^{-4}
Mean				**0.049 ± 0.001**					0.063	**$4.3 \pm 1.1 \times 10^{-4}$**
LC #1	24 hours	84.0%	1295	0.049	$E = 0.03342\tau_0 - 0.00007$	0.97	0.6	Type II	0.068	6.3×10^{-4}
LC #2	24 hours	82.9%	1313	0.051	$E = 0.02214\tau_0 - 0.00005$	0.99	0.4	Type II	0.070	3.8×10^{-4}
LC #3	24 hours	83.5%	1304	0.052	$E = 0.02119\tau_0 - 0.00005$	0.96	0.4	Type II	0.075	4.0×10^{-4}
LC #4	24 hours	83.1%	1310	0.049	$E = 0.01999\tau_0 - 0.00003$	0.96	0.4	Type II	0.069	3.6×10^{-4}
LC #5	24 hours	83.5%	1304	0.049	$E = 0.01772\tau_0 - 0.00007$	0.97	0.5	Type II	0.076	3.9×10^{-4}
LC #6	24 hours	83.1%	1310	0.052	$E = 0.01800\tau_0 - 0.00002$	0.99	0.5	Type II	0.075	4.0×10^{-4}
LC #7*	24 hours	82.7%	1316	0.050	$E = 0.01342\tau_0 - 0.00003$	0.99	0.5	Type II	0.069	2.3×10^{-4}
Mean				**0.050 ± 0.001**					0.072	**$4.0 \pm 1.1 \times 10^{-4}$**
LC #8	1 month	83.6%	1301	0.057	$E = 0.00006\ln(\tau_0) + 0.00033$	0.99	0.4	Type II	0.101	1.5×10^{-4}

Table 3. Summary of experiments studying the mobility of variable-porosity ooze. Indicated are different observed erosion types during each experiment along with different total bed porosity φ and wet bulk density ρ_b. Erosion threshold τ_c indicates onset of a particular erosion type. Erosion rate E_m is given as an average at the maximum applied shear stress τ_{0max}. Erosion depth z_e is given at the end of the velocity step at applied τ_{0max}.

Run	φ	ρ_b (kg/m^3)	τ_c *(Pa)*	z_e *(mm)*	Erosion type	τ_{0max} *(Pa)*	E_m *(kg/m^2/s)*
MF #7	82.2%	1325	0.061	0.03	Type II s	0.076	2.7 x 10^{-5}
			0.082	0.22	Type I/II	0.103	3.9 x 10^{-4}
MF #8	80.7%	1350	0.063	0.01	Type II s	0.076	7.4 x 10^{-6}
			0.084	0.15	Type I/II	0.103	3.0 x 10^{-4}
			0.112	0.24	Type II	0.121	9.8 x 10^{-4}
MF #9	79.2%	1375	0.061	0.03	Type II s	0.076	2.7 x 10^{-5}
			0.082	0.23	Type I/II	0.121	4.8 x 10^{-4}
MF #10	77.7%	1400	0.068	0.004	Type II s	0.085	6.0 x 10^{-6}
			0.092	0.05	Type I/II	0.121	5.7 x 10^{-5}
			0.129	0.19	Type III	0.157	7.8 x 10^{-4}
MF #11	76.3%	1425	0.070	0.005	Type I s	0.085	6.1 x 10^{-6}
			0.091	0.04	Type I/II	0.121	3.9 x 10^{-5}
			0.130	0.08	Type II	0.139	9.5 x 10^{-5}
			0.148	0.20	Type III	0.157	4.6 x 10^{-4}
MF #12	74.8%	1450	0.074	0.005	Type I s	0.085	6.8 x 10^{-6}
			0.094	0.04	Type I/II	0.121	5.3 x 10^{-5}
			0.130	0.09	Type II	0.139	1.3 x 10^{-4}
			0.148	0.19	Type III	0.157	5.5 x 10^{-4}
MF #13	73.3%	1475	0.069	0.009	Type I s	0.085	1.1 x 10^{-5}
			0.094	0.05	Type I/II	0.121	6.1 x 10^{-5}
			0.130	0.13	Type II	0.139	1.9 x 10^{-4}
			0.148	0.21	Type III	0.157	5.0 x 10^{-4}
MF #14	71.8%	1500	0.081	0.003	Type I s	0.085	3.4 x 10^{-6}
			0.097	0.03	Type I/II	0.139	3.7 x 10^{-5}
			0.148	0.07	Type II	0.157	9.5 x 10^{-5}
			0.166	0.20	Type III	0.175	4.8 x 10^{-4}
MF #15	68.8%	1550	0.081	0.003	Type I s	0.085	4.8 x 10^{-6}
			0.097	0.03	Type I/II	0.139	3.8 x 10^{-5}
			0.148	0.06	Type II	0.157	7.3 x 10^{-5}
			0.166	0.16	Type III	0.175	2.5 x 10^{-4}
MF #16	65.9%	1600	0.081	0.005	Type I s	0.085	6.1 x 10^{-6}
			0.096	0.06	Type I/II	0.157	5.5 x 10^{-5}
			0.166	0.10	Type II	0.175	9.9 x 10^{-5}
			0.184	0.18	Type III	0.193	3.5 x 10^{-4}
MF #17	59.9%	1700	0.081	0.006	Type I s	0.085	6.3 x 10^{-6}
			0.094	0.05	Type I/II	0.175	2.7 x 10^{-5}
			0.186	0.08	Type II	0.211	5.5 x 10^{-5}
			0.221	0.16	Type III	0.229	1.7 x 10^{-4}

Table 4. Summary of observed mass settling velocities W_s, equivalent sedimentation diameter D_s (calculated for calcite with ρ_s of 2710 kg/m^3), and estimated deposition thresholds τ_{cd} during the depositional phase of the experiment. Bed porosity φ and wet bulk density ρ_b given for initial beds from which the material was eroded during the erosion phase of the experiment, prior to the deposition phase. Indicated maximum suspended sediment concentration SSC_{max} that was reached at the maximum applied shear stress τ_{0max}. Run LC #7 is with 20 min step length. Run LC #8 is a high-porosity bed after 1 month of consolidation. * indicates runs on a smooth flume floor without sediment cover.

Run	φ	ρ_b (kg/m^3)	τ_{cd} (Pa)	W_s (m/s)	D_s, µm	τ_{0max} (Pa)	SSC_{max} (g/l)
MF #3	84.9%	1280	0.037	8.9×10^{-4}	33	0.058	1.8
MF #6	84.9%	1280	0.037	6.0×10^{-4}	27	0.063	1.6
LC #6	83.1%	1310	0.047	9.5×10^{-4}	34	0.075	1.6
LC #7	82.7%	1316	0.049	5.9×10^{-4}	26	0.069	1.7
LC #8	83.6%	1301	0.059	5.4×10^{-4}	25	0.101	1.6
MF #7	82.2%	1325	0.068	4.3×10^{-4}	23	0.103	1.4
MF #8	80.7%	1350	0.067	5.7×10^{-4}	26	0.121	1.4
MF #9	79.2%	1375	0.071	4.4×10^{-4}	23	0.121	1.4
MF #10	77.7%	1400	0.095	4.1×10^{-4}	22	0.157	1.4
MF #11	76.3%	1425	0.093	4.4×10^{-4}	23	0.157	1.4
MF #12	74.8%	1450	0.089	4.3×10^{-4}	23	0.157	1.4
MF #13	73.3%	1475	0.095	5.0×10^{-4}	24	0.157	1.5
MF #14	71.8%	1500	0.096	4.0×10^{-4}	22	0.175	1.4
MF #15	68.8%	1550	0.104	3.4×10^{-4}	20	0.175	1.4
MF #16	65.9%	1600	0.128	3.3×10^{-4}	20	0.193	1.4
MF #17	59.9%	1700	0.125	3.1×10^{-4}	19	0.229	1.5
LC#9				7.1×10^{-4}	29		
LC#10*			0.062	6.4×10^{-4}	28	0.239	0.9
LC#11				5.9×10^{-4}	27		
LC#12*			0.079	9.5×10^{-4}	34	0.239	1.7
LC#13				1.1×10^{-3}	37		